

Fock-space perturbed relativistic coupled-cluster calculations of electric dipole polarizability and nuclear spin-dependent parity non-conservation in Cs

Suraj Pandey,¹ Ravi Kumar,² D. Angom,³ and B. K. Mani^{1,*}

¹*Department of Physics, Indian Institute of Technology, Hauz Khas, New Delhi 110016, India*

²*Department of Chemistry, University of Zurich, Switzerland*

³*Department of Physics, Manipur University, Canchipur 795003, Manipur, India*

We implement the Fock-space perturbed relativistic coupled-cluster theory to compute the electric dipole polarizability of ground and low lying excited states, and nuclear spin-dependent parity violating (NSD-PNC) transition amplitudes in Cs. Moreover, to check the accuracy of the wavefunctions used in the calculations, we compute the excitation energies, E1 transition amplitudes and magnetic dipole hyperfine constants for ground and low lying excited states. To improve the accuracy of the computed properties, we have incorporated the corrections from the relativistic and QED effects in our calculations. The contributions from triple excitations are accounted perturbatively. Our results on excitation energies, E1 transition amplitudes and hyperfine constants are in good agreement with the available experimental results. Our polarizability results using FS-PRCC theory match well with the experimental values. The values of parity-violating transition amplitudes from our calculations are, in general, on the lower side of the previous values. From the detail analysis of electron correlations, we find that the corrections from the Breit interaction and QED effects are important to get accurate results of NSD-PNC amplitudes in Cs. The largest cumulative contribution from the Breit and QED corrections is found to be $\approx 3.2\%$ of the total value. The upper bound on the theoretical uncertainty in our calculated NSD-PNC amplitudes is estimated to be about 1%.

I. INTRODUCTION

The parity nonconservation (PNC) in atoms and ions is one of the most important phenomena in fundamental physics to understand physics beyond the Standard Model of particle physics [1, 2]. The PNC in atoms manifest in two forms, nuclear spin-independent (NSI) and nuclear spin-dependent (NSD). The NSI-PNC is well studied both experimentally [3–5] as well as theoretically [6–9] in several atoms. To date, the most precise PNC measurement was carried out using Cs atom at Colorado by Wood *et. al.* [5] with an accuracy of 0.35%. The most precise theoretical results also correspond to Cs, where the reported NSI-PNC amplitude is calculated with a theoretical accuracy of 0.27% [6, 10]. Unlike NSI-PNC, the NSD-PNC is not well explored. The same Cs experiment [5] also observed a signature of NSD-PNC but the effect was very weak due to strong NSI-PNC component. The experimental error in the reported NSD-PNC observable was $\approx 15\%$ [5]. In theoretical studies too, it is challenging to compute NSD-PNC transition amplitudes accurately as it involves coupling of nuclear and electronic wavefunctions. It is, however, important to explore NSD-PNC in atomic systems as it is essential to deduce nuclear properties like the anapole moment (NAM). The NAM, first suggested by Zeldovich [11], is a parity odd nuclear electromagnetic moment and arises from parity violating phenomena within the nucleus. It should be noted that, NAM is one of the dominant sources to NSD-PNC. The other two sources are, the combination of hyperfine and nuclear spin-independent PNC and spin-dependent Z-exchange between electrons and nucleus.

As theoretical results are essential to obtain NAM from the experimental data, it is crucial to employ reliable and accurate

quantum many-body theory in the calculations. The theory must account for electron correlations and relativistic effects to the highest possible level of accuracy. Among the previous theoretical works on calculations of NSD-PNC transition amplitudes in Cs, there are two calculations which use methods significantly different from the present work. The first one is by Johnson and collaborators [12], they used random-phase-approximation (RPA). And, the second one by Safronova and collaborators [13] uses all-order method. There are two other works [14, 15] using methods similar to the present work. Although the two calculations employ similar coupled-cluster method, there is a difference in the reported values of the transition amplitudes. An important point to be highlighted is, none of the previous works incorporate corrections from the Breit interaction, QED effects and triples excitations in coupled-cluster. It should, however, be noted that these corrections are important to get accurate and reliable values of parity violating transition amplitudes. It can thus be surmised that the availability of accurate theoretical data on NSD-PNC in Cs is a research gap which needs to be addressed. Addressing this gap is one of the main aims of the present work

In this work, we implement a Fock-space perturbed relativistic coupled-cluster (FS-PRCC) theory to compute NSD-PNC electric dipole transition amplitude, $E1_{\text{PNC}}^{\text{NSD}}$, for all allowed hyperfine transitions corresponding to the $6s_{1/2} \rightarrow 7s_{1/2}$ transition in Cs. It is to be noted that, relativistic coupled-cluster (RCC) theory is one of the most reliable many-body theories for atomic structure calculations. It accounts for the electron correlations to all-orders of residual Coulomb interaction, and has been employed to study a plethora of properties in atomic systems. The implementation of RCC theory including properties calculations of closed-shell and one-valence atomic systems without perturbation is reported in our previous work [16]. For properties calculation in the presence of external perturbation, we had reported the development of PRCC theory for closed-shell and one-valence

* bkmani@physics.iitd.ac.in

systems in our previous works [17–21]. A PRCC theory for PNC calculation is reported in our recent work [22]. One of the key merits of PRCC in properties calculation is that it does not employ the sum-over-states approach [23, 24] to incorporate the effects of perturbation. In PRCC, summation over all the possible intermediate states is subsumed through the perturbed cluster operators.

Furthermore, to check the accuracy of the wavefunctions in the small and large r regions, we calculate the hyperfine constants and E1 transition amplitudes, respectively. In addition, to check and validate our implementation of PRCC theory for NSD-PNC, we compute the dipole polarizability, α , of ground state $6s_{1/2}$ and PNC-transition state $7s_{1/2}$ using PRCC. Except for the angular factor, as the coupled-cluster diagrams for PNC are similar to the polarizability diagrams obtaining accurate α using PRCC indicates possibility of obtaining accurate $E1_{\text{PNC}}^{\text{NSD}}$. To verify the results, we also use the sum-over-states approach to compute α for $6s_{1/2}$, $6p_{1/2}$, $7s_{1/2}$ and $7p_{1/2}$ states. The other key highlight of the present work is, to further improve the accuracy of our results, we have incorporated the corrections from the Breit interaction, QED effects and perturbative triples in the calculation.

The remainder of the paper is divided into five sections. In Sec. II, we provide a brief discussion on the FSRCC and FS-PRCC theories for one-valence systems. In the same section, we also elaborate the calculation of $E1_{\text{PNC}}^{\text{NSD}}$ using FS-PRCC theory and discuss the corresponding Goldstone diagrams. Then, the coupling of nuclear spin with the electronic states is also discussed in the same section. In Sec. III, we present and discuss our results of excitation energy, E1 transition amplitudes and hyperfine constants, dipole polarizability, and $E1_{\text{PNC}}^{\text{NSD}}$ in different subsections. The theoretical uncertainty is presented in Sec. IV of the paper. Unless stated otherwise, all the results and equations presented in the paper are in atomic units ($\hbar = m_e = e = 1/4\pi\epsilon_0 = 1$).

II. THEORETICAL METHODS

A. FSRCC theory for one-valence systems

To obtain accurate results in the structure or property calculations of an atom or ion, it is essential to use accurate wavefunctions. In the present work, we have used FSRCC theory for one-valence [16, 25] to compute many-body wavefunctions and the corresponding energies for the ground and low-lying excited states of Cs atom. Here, we briefly discuss the theory used in our calculations. For a one-valence atom or ion, the many-body wavefunction is the solution of the eigenvalue equation

$$H^{\text{DCB}}|\Psi_v\rangle = E_v|\Psi_v\rangle, \quad (1)$$

where $|\Psi_v\rangle$ is the exact wavefunction with the corresponding energy E_v and H^{DCB} is the Dirac-Coulomb-Breit no-virtual-

pair Hamiltonian. For an atom or ion with N -electrons

$$H^{\text{DCB}} = \Lambda_{++} \sum_{i=1}^N [c\alpha_i \cdot \mathbf{p}_i + (\beta_i - 1)c^2 - V_N(r_i)] + \sum_{i<j} \left[\frac{1}{r_{ij}} + g^{\text{B}}(r_{ij}) \right] \Lambda_{++}, \quad (2)$$

where α and β are the Dirac matrices, and $V_N(r_i)$ is the nuclear potential. The last two terms, $1/r_{ij}$ and $g^{\text{B}}(r_{ij})$, are the Coulomb and Breit interactions, respectively. For Breit interaction, we employ the expression [26]

$$g^{\text{B}}(r_{12}) = -\frac{1}{2r_{12}} \left[\alpha_1 \cdot \alpha_2 + \frac{(\alpha_1 \cdot \mathbf{r}_{12})(\alpha_2 \cdot \mathbf{r}_{12})}{r_{12}^2} \right]. \quad (3)$$

The operator Λ_{++} projects onto the positive-energy solutions, and therefore, sandwiching the Hamiltonian between Λ_{++} ensures that the effects of the negative-energy continuum states are neglected in the present calculations.

In the coupled-cluster (CC) theory, the wavefunction $|\Psi_v\rangle$ is expressed in terms of the cluster operators as

$$|\Psi_v\rangle = e^{T^{(0)}} [1 + S^{(0)}] |\Phi_v\rangle, \quad (4)$$

where $T^{(0)}$ and $S^{(0)}$ represent the unperturbed cluster operators for closed-shell and one-valence sectors, respectively. The state $|\Phi_v\rangle$ is the Dirac-Fock reference state for one-valence system. It is obtained by adding a valence-electron to the closed-shell reference state $|\Phi_0\rangle$ using the creation operator a_v^\dagger as $|\Phi_v\rangle = a_v^\dagger |\Phi_0\rangle$. In the coupled-cluster with singles and doubles (CCSD) approximation, the $T^{(0)}$ and $S^{(0)}$ operators are defined as $T^{(0)} = T_1^{(0)} + T_2^{(0)}$ and $S^{(0)} = S_1^{(0)} + S_2^{(0)}$, respectively. The expressions of these operators in the second quantized form are

$$T_1^{(0)} = \sum_{a,p} t_a^p a_p^\dagger a_a, \quad T_2^{(0)} = \frac{1}{2!} \sum_{a,b,p,q} t_{ab}^{pq} a_p^\dagger a_q^\dagger a_b a_a, \quad (5a)$$

$$S_1^{(0)} = \sum_p s_p^p a_p^\dagger a_v, \quad S_2^{(0)} = \sum_{a,p,q} s_{va}^{pq} a_p^\dagger a_q^\dagger a_a a_v. \quad (5b)$$

Here, t_{\dots} and s_{\dots} represent the cluster amplitudes and the indices a, b, c, \dots (p, q, r, \dots) represent the core (virtual) states and v, w, x, \dots represent the valence orbitals. The operators T_1 (S_1) and T_2 (S_2) generate single and double electron replacements after operating on the closed(open)-shell reference states. The diagrammatic representation of these operators are shown in Fig. 1. The open-shell CC operators $S_1^{(0)}$ and $S_2^{(0)}$ are obtained by solving the coupled linear equations [16, 25]

$$\langle \Phi_v^p | \bar{H}_N + \{ \bar{H}_N S^{(0)} \} | \Phi_v \rangle = E_v^{\text{att}} \langle \Phi_v^p | S_1^{(0)} | \Phi_v \rangle, \quad (6a)$$

$$\langle \Phi_{va}^{pq} | \bar{H}_N + \{ \bar{H}_N S^{(0)} \} | \Phi_v \rangle = E_v^{\text{att}} \langle \Phi_{va}^{pq} | S_2^{(0)} | \Phi_v \rangle. \quad (6b)$$

Here, $H_N = H^{\text{DCB}} - \langle \Phi_0 | H^{\text{DCB}} | \Phi_0 \rangle$ is the normal ordered Hamiltonian and $\bar{H}_N = e^{-T^{(0)}} H_N e^{T^{(0)}}$ is a similarity transformed Hamiltonian. The energy E_v^{att} is the attachment energy of the valence electron, expressed as $E_v^{\text{att}} = \epsilon_v + \Delta E_v$,

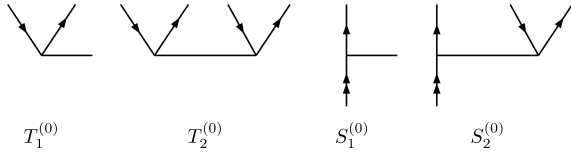


FIG. 1. Diagrammatic representation of the unperturbed single and double CC operators for closed-shell and one-valence sectors.

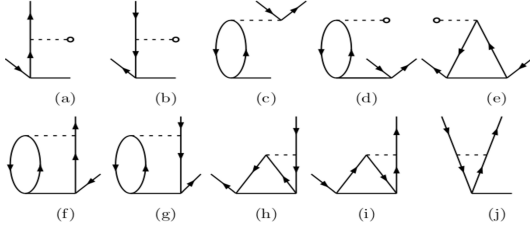


FIG. 2. The Goldstone diagrams contributing to the linearized unperturbed CC equation of $T_1^{(0)}$. Diagrams contributing to CC equation of $S_1^{(0)}$ can be obtained by converting *core* line to *valence* line. Dashed lines *with* and *without*-circle represent the *one*- and *two*-body Coulomb interactions, respectively.

where ϵ_v is the single-particle energy and ΔE_v is the correlation energy. Similarly, the closed-shell CC operators $T_1^{(0)}$ and $T_2^{(0)}$ are the solutions of coupled nonlinear equations [16, 27]

$$\langle \Phi_a^p | \bar{H}_N | \Phi_0 \rangle = 0, \quad (7a)$$

$$\langle \Phi_{ab}^{pq} | \bar{H}_N | \Phi_0 \rangle = 0. \quad (7b)$$

Here, $|\Phi_a^p\rangle$ and $|\Phi_{ab}^{pq}\rangle$ represent the Slater determinants with single and double excitations. In the Figs. 2 and 3, we have shown the CC diagrams of the *linearized* RCC theory for closed-shell atoms corresponding to the $T_1^{(0)}$ and $T_2^{(0)}$ equations, respectively. The diagrams corresponding to $S_1^{(0)}$ and $S_2^{(0)}$ can be obtained by converting one of the *core* lines to *valence* line.

B. FS-PRCC theory of PNC for one-valence systems

In the presence of NSD-PNC interaction, the atomic Hamiltonian is modified to

$$H_t = H^{\text{DCB}} + \lambda H_{\text{PNC}}, \quad (8)$$

where λ is a perturbation parameter and $H_{\text{PNC}}^{\text{NSD}}$ is the NSD-PNC interaction Hamiltonian with the expression

$$H_{\text{PNC}}^{\text{NSD}} = \frac{G_F \mu'_W}{\sqrt{2}} \sum_i \alpha_i \cdot \mathbf{I} \rho_N(r), \quad (9)$$

where, $G_F = 2.22 \times 10^{-14}$ a.u. is the Fermi coupling constant, μ'_W is the weak nuclear moment of the nucleus, α is the

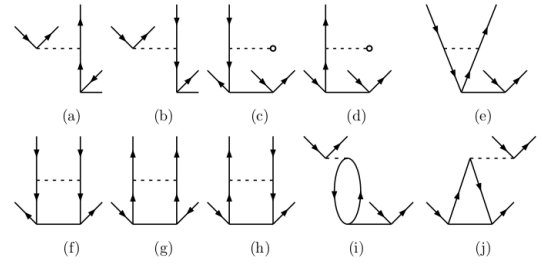


FIG. 3. The Goldstone diagrams contributing to the linearized unperturbed CC equation of $T_2^{(0)}$. Diagrams contributing to CC equation of $S_2^{(0)}$ can be obtained by converting one of *core* lines to a *valence* line. Dashed lines *with* and *without*-circle represent the *one*- and *two*-body Coulomb interactions, respectively.

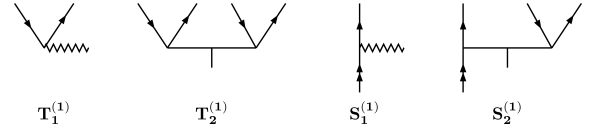


FIG. 4. Diagrammatic representations of NSD-perturbed cluster operators in closed-shell and one-valence sectors. The extra line in $T_2^{(1)}$ and $S_2^{(1)}$ is to indicate the multipole structure of the operators.

Dirac matrix, and \mathbf{I} and $\rho_N(r)$ are the nuclear spin and density, respectively. Defining $H_{\text{elec}}^{\text{NSD}} = (G_F \mu'_W / \sqrt{2}) \sum_i \alpha_i \rho_N(r)$, the interaction Hamiltonian can be written in the compact form

$$H_{\text{PNC}}^{\text{NSD}} = \mathbf{H}_{\text{elec}}^{\text{NSD}} \cdot \mathbf{I}. \quad (10)$$

Due to $H_{\text{PNC}}^{\text{NSD}}$ the atomic states mix with opposite parity states, and hence, these are no longer parity eigen states. We refer to these mixed parity states as perturbed states and are solutions of the eigen value equation

$$H_t |\tilde{\Psi}_v\rangle = \tilde{E}_v |\tilde{\Psi}_v\rangle, \quad (11)$$

where \tilde{E}_v is the perturbed eigen energy. To first-order in λ , $|\tilde{\Psi}_v\rangle = |\Psi_v\rangle + \lambda |\bar{\Psi}_v^1\rangle$ and $\tilde{E}_v = E_v + \lambda E_v^1$, where the bar in $|\bar{\Psi}_v^1\rangle$ denotes a state opposite in parity to $|\Psi_v\rangle$. Using Eqs. (8) and (9) in Eq. (11), we obtain

$$(H^{\text{DCB}} + \lambda \mathbf{H}_{\text{elec}}^{\text{NSD}} \cdot \mathbf{I}) |\tilde{\Psi}_v\rangle = E_v |\tilde{\Psi}_v\rangle. \quad (12)$$

Here, we have used $E_v^1 = \langle \Psi_v | H_{\text{PNC}}^{\text{NSD}} | \Psi_v \rangle = 0$, as $H_{\text{PNC}}^{\text{NSD}}$ is an odd parity operator it connects only to states with opposite parities. The presence of nuclear spin operator \mathbf{I} in NSD-PNC Hamiltonian leads to two important considerations. First, the cluster operators in the electronic sector are rank one operators. And second, atomic states are the eigenstates of the total angular momentum operator $\mathbf{F} = \mathbf{I} + \mathbf{J}$.

In FS-PRCC theory, the perturbed wavefunction is written as

$$|\tilde{\Psi}_v\rangle = e^{T^{(0)}} \left[1 + \lambda \mathbf{T}^{(1)} \cdot \mathbf{I} \right] \left[1 + S^{(0)} + \lambda \mathbf{S}^{(1)} \cdot \mathbf{I} \right] |\Phi_v\rangle, \quad (13)$$

where $\mathbf{T}^{(1)}$ and $\mathbf{S}^{(1)}$ are the closed-shell and one-valence perturbed operators, respectively. Here, the superscript (1) is used to indicate that the clusters subsume the perturbation. Similar to the case of unperturbed operators $T^{(0)}$ and $S^{(0)}$, in the CCSD approximation, we consider $\mathbf{T}^{(1)} = \mathbf{T}_1^{(1)} + \mathbf{T}_2^{(1)}$ and $\mathbf{S}^{(1)} = \mathbf{S}_1^{(1)} + \mathbf{S}_2^{(1)}$. Since these are tensor operators, they satisfy selection rules which are different from the unperturbed cluster operators. The second quantized tensorial representation of $\mathbf{T}^{(1)}$ is described in detail in one of our previous works [20]. Here we discuss the second quantized representation and selection rules for the operator $\mathbf{S}^{(1)}$. In the second quantized notation

$$\mathbf{S}_1^{(1)} = \sum_p \xi_v^p \mathbf{C}_1(\hat{r}) a_p^\dagger a_v, \quad (14a)$$

$$\mathbf{S}_2^{(1)} = \sum_{apq} \sum_{lk} \xi_{va}^{pq}(l, k) \mathbf{C}_l(\hat{r}_1) \mathbf{C}_k(\hat{r}_2) a_p^\dagger a_q^\dagger a_a a_v. \quad (14b)$$

Here, ξ_{\dots} represents the cluster amplitude for the operator $\mathbf{S}^{(1)}$. The one-body operator $\mathbf{S}_1^{(1)}$ is an odd parity operator and expressed in terms of a rank-one \mathbf{C} -tensor. It satisfies the parity and triangular selection rules $(-1)^{l_v+l_p} = -1$ and

$|j_v - j_p| \leq 1 \leq (j_v + j_p)$. The tensor structure of the two-body operator $\mathbf{S}_2^{(1)}$ involves two \mathbf{C} -tensors of ranks l and k associated with its two-vertices. These two \mathbf{C} -tensors couple to give a rank-one operator, $\mathbf{S}_2^{(1)}$. The selection rules of $\mathbf{S}_2^{(1)}$ are $(-1)^{l_v+l_p} = -(-1)^{l_a+l_q}$ and $|j_v - j_p| \leq l \leq (j_v + j_p)$, $|j_a - j_q| \leq k \leq (j_a + j_q)$. The diagrammatic representations of $\mathbf{T}^{(1)}$ and $\mathbf{S}^{(1)}$ are shown in Fig. 4.

Using Eq. (13) in Eq. (12) and projecting entire equation on $e^{-T^{(0)}}$ from left and retaining the terms linear in λ , we get

$$\begin{aligned} & \left[\bar{H}_N \mathbf{S}^{(1)} + \bar{H}_N \mathbf{T}^{(1)} (1 + S^{(0)}) + \bar{\mathbf{H}}_{\text{elec}}^{\text{NSD}} (1 + S^{(0)}) \right] |\Phi_v\rangle \\ & = \left[\Delta E_v \mathbf{S}^{(1)} + \Delta E_v \mathbf{T}^{(1)} (1 + S^{(0)}) \right] |\Phi_v\rangle. \end{aligned} \quad (15)$$

Here, $\Delta E_v = E_v - \langle \Phi_v | H^{\text{DCB}} | \Phi_v \rangle$ is the correlation energy of the one-valence system. And, like \bar{H}_N introduced earlier, $\bar{\mathbf{H}}_{\text{elec}}^{\text{NSD}} = e^{-T^{(0)}} \mathbf{H}_{\text{elec}}^{\text{NSD}} e^{T^{(0)}}$ is the similarity transformed PNC Hamiltonian in the electronic space. The PRCC equations of the $\mathbf{S}_1^{(1)}$ and $\mathbf{S}_2^{(1)}$ can be obtained by projecting Eq. (15) with single and double excited determinants $\langle \Phi_v^p |$ and $\langle \Phi_{va}^{pq} |$, respectively, as

$$\langle \Phi_v^p | \{ \bar{H}_N \mathbf{S}^{(1)} \} + \{ \bar{H}_N \mathbf{T}^{(1)} \} + \{ \bar{H}_N \mathbf{T}^{(1)} S^{(0)} \} + \bar{\mathbf{H}}_{\text{elec}}^{\text{NSD}} + \{ \bar{\mathbf{H}}_{\text{elec}}^{\text{NSD}} S^{(0)} \} | \Phi_v \rangle = E_v^{\text{att}} \langle \Phi_v^p | \mathbf{S}_1^{(1)} | \Phi_v \rangle, \quad (16a)$$

$$\langle \Phi_{va}^{pq} | \{ \bar{H}_N \mathbf{S}^{(1)} \} + \{ \bar{H}_N \mathbf{T}^{(1)} \} + \{ \bar{H}_N \mathbf{T}^{(1)} S^{(0)} \} + \bar{\mathbf{H}}_{\text{elec}}^{\text{NSD}} + \{ \bar{\mathbf{H}}_{\text{elec}}^{\text{NSD}} S^{(0)} \} | \Phi_v \rangle = E_v^{\text{att}} \langle \Phi_{va}^{pq} | \mathbf{S}_2^{(1)} | \Phi_v \rangle. \quad (16b)$$

In deriving the above equations we have used the relations, $\langle \Phi_v^p | \mathbf{T}^{(1)} | \Phi_v \rangle = 0$ and $\langle \Phi_v^p | \mathbf{T}^{(1)} S^{(0)} | \Phi_v \rangle = 0$. These follow because $\mathbf{T}^{(1)}$, as an operator of closed-shell sector, does not contribute to the PRCC equation of $\mathbf{S}_1^{(1)}$ and $\mathbf{S}_2^{(1)}$. The closed-shell perturbed operators $\mathbf{T}^{(1)}$ are the solutions of a similar set of coupled equations [20, 27]

$$\langle \Phi_a^p | \{ \bar{H}_N \mathbf{T}^{(1)} \} | \Phi_0 \rangle = -\langle \Phi_a^p | \bar{\mathbf{H}}_{\text{elec}}^{\text{NSD}} - \Delta E_0 \mathbf{T}^{(1)} | \Phi_0 \rangle, \quad (17a)$$

$$\langle \Phi_{ab}^{pq} | \{ \bar{H}_N \mathbf{T}^{(1)} \} | \Phi_0 \rangle = -\langle \Phi_{ab}^{pq} | \bar{\mathbf{H}}_{\text{elec}}^{\text{NSD}} - \Delta E_0 \mathbf{T}^{(1)} | \Phi_0 \rangle, \quad (17b)$$

where ΔE_0 is the correlation energy of closed-shell sector of the atom. In Figs. 5 and 6, we have shown the CC diagrams for $\mathbf{T}_1^{(1)}$ and $\mathbf{T}_2^{(1)}$ which contribute to the *linearized* PRCC theory. The corresponding diagrams for $\mathbf{S}_1^{(1)}$ and $\mathbf{S}_2^{(1)}$ are ob-

tained by transforming one of the *core* lines to a *valence* line.

C. Calculation of $E1_{\text{PNC}}^{\text{NSD}}$ using FS-PRCC theory

The PNC induced electric dipole transition amplitude $E1_{\text{PNC}}^{\text{NSD}}$ is the transition matrix element of the dipole operator \mathbf{D} between the initial and final perturbed states

$$E1_{\text{PNC}}^{\text{NSD}} = \frac{\langle \tilde{\Psi}_w | \mathbf{D} | \tilde{\Psi}_v \rangle}{\sqrt{\langle \tilde{\Psi}_v | \tilde{\Psi}_v \rangle} \sqrt{\langle \tilde{\Psi}_w | \tilde{\Psi}_w \rangle}}. \quad (18)$$

The advantage with this expression is that, unlike the often used sum-over-states approach [28], it implicitly accounts for all possible intermediate states. Using Eq. (13) in (18) and retaining terms up to second order in CC operators, we can write the electronic component of $E1_{\text{PNC}}^{\text{NSD}}$, with the CCSD approximation, as

$$\begin{aligned} E1_{\text{elec}}^{\text{NSD}} \approx & \frac{1}{\mathcal{N}} \langle \Phi_w | \left(\mathbf{D} \mathbf{S}_1^{(1)} + \mathbf{D} \mathbf{S}_2^{(1)} + \mathbf{S}_1^{(0)\dagger} \mathbf{D} \mathbf{S}_1^{(1)} + \mathbf{S}_1^{(0)\dagger} \mathbf{D} \mathbf{S}_2^{(1)} + \mathbf{S}_2^{(0)\dagger} \mathbf{D} \mathbf{S}_1^{(1)} + \mathbf{S}_2^{(0)\dagger} \mathbf{D} \mathbf{S}_2^{(1)} + \mathbf{S}_1^{(0)\dagger} \mathbf{D} \mathbf{T}_1^{(1)} + \mathbf{S}_2^{(0)\dagger} \mathbf{D} \mathbf{T}_1^{(1)} \right. \\ & + \mathbf{S}_2^{(0)\dagger} \mathbf{D} \mathbf{T}_2^{(1)} + \mathbf{T}_1^{(0)\dagger} \mathbf{D} \mathbf{S}_1^{(1)} + \mathbf{T}_1^{(0)\dagger} \mathbf{D} \mathbf{S}_2^{(1)} + \mathbf{T}_2^{(0)\dagger} \mathbf{D} \mathbf{S}_2^{(1)} + \mathbf{D} \mathbf{T}^{(1)} + \mathbf{T}_1^{(0)\dagger} \mathbf{D} \mathbf{T}_1^{(1)} + \mathbf{T}_1^{(0)\dagger} \mathbf{D} \mathbf{T}_2^{(1)} + \mathbf{T}_2^{(0)\dagger} \mathbf{D} \mathbf{T}_1^{(1)} \\ & \left. + \mathbf{T}_2^{(0)\dagger} \mathbf{D} \mathbf{T}_2^{(1)} \right) + \text{H.c.} + \mathbf{D} \mathbf{T}_1^{(1)} S_1^{(0)} + \mathbf{D} \mathbf{T}_1^{(1)} S_1^{(0)} | \Phi_v \rangle. \end{aligned} \quad (19)$$

Here,

$$\begin{aligned} \mathcal{N} = & \sqrt{\langle \Phi_v | (e^{T^{(0)}} (1 + S^{(0)}))^\dagger (e^{T^{(0)}} (1 + S^{(0)})) | \Phi_v \rangle} \\ & \times \sqrt{\langle \Phi_w | (e^{T^{(0)}} (1 + S^{(0)}))^\dagger (e^{T^{(0)}} (1 + S^{(0)})) | \Phi_w \rangle}, \end{aligned} \quad (20)$$

is the normalization factor. The terms $\mathbf{S}_1^{(0)\dagger} \mathbf{D} \mathbf{T}_2^{(1)} + \text{H.c.}$,

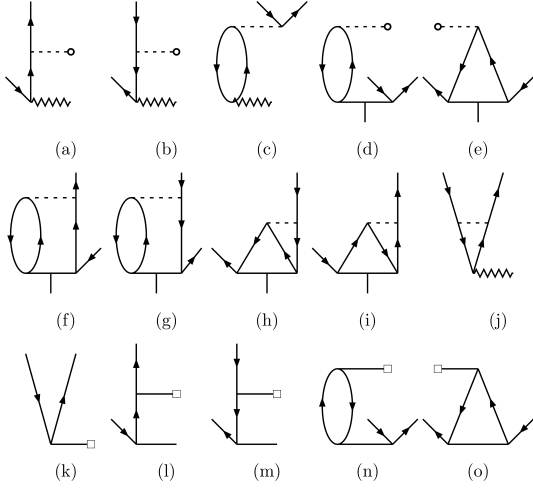


FIG. 5. The Goldstone diagrams which contribute to the linearized perturbed CC equations of $\mathbf{T}_1^{(1)}$. The diagrams for $\mathbf{S}_1^{(1)}$ can be obtained by converting *core* line to the *valence* line. The dashed lines *with* and *without*-circle represent the *one*- and *two*-body Coulomb interactions, respectively. The bar with square represents the PNC operator.

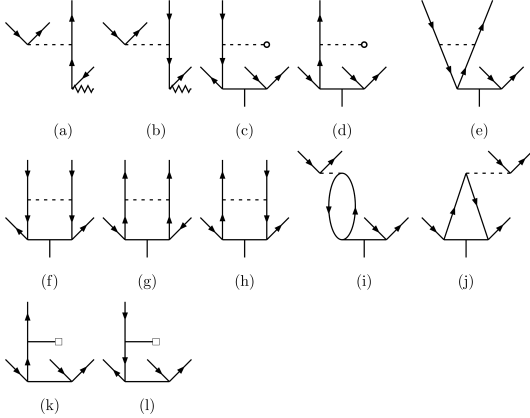


FIG. 6. The Goldstone diagrams which contribute to the linearized perturbed CC equations of $\mathbf{T}_2^{(1)}$. The diagrams for $\mathbf{S}_2^{(1)}$ can be obtained by converting *core* line to the *valence* line. The dashed lines *with* and *without*-circle represent the *one*- and *two*-body Coulomb interactions, respectively. The bar with square represents the PNC operator.

$T_2^{(0)\dagger} \mathbf{DS}_2^{(1)} + \text{H.c.}$ and $\mathbf{DT}_2^{(1)} + \text{H.c.}$ are not included as these do not contribute to $E1_{\text{elec}}^{\text{NSD}}$ for one-valence system.

As evident, the expression in Eq. (19) is independent of the nuclear spin, and hence can be computed within the electronic space alone. To evaluate this, we use Goldstone diagrams to identify the contributing terms, and these are then evaluated using the diagrammatic techniques [29]. As demonstrated in our previous work [25], the diagrams arising from terms with cubic or higher orders of CC operators have negligible contributions, so they are not included in the equation. There are 128 Goldstone diagrams which contribute to Eq. (19) and, as

an example, we show one diagram from each of the terms in Eq. (19) in Fig. 7. The diagrams from the Hermitian conjugate terms are not shown as these are topologically equivalent. Among all the terms, the first two terms $\mathbf{DS}_1^{(1)}$ and $\mathbf{DS}_2^{(1)}$, and their Hermitian conjugates, are expected to have the dominant contribution to $E1_{\text{elec}}^{\text{NSD}}$. The reason for this can be attributed to the larger magnitudes of the one-valence CC operators and the strong effect of perturbation on these operators.

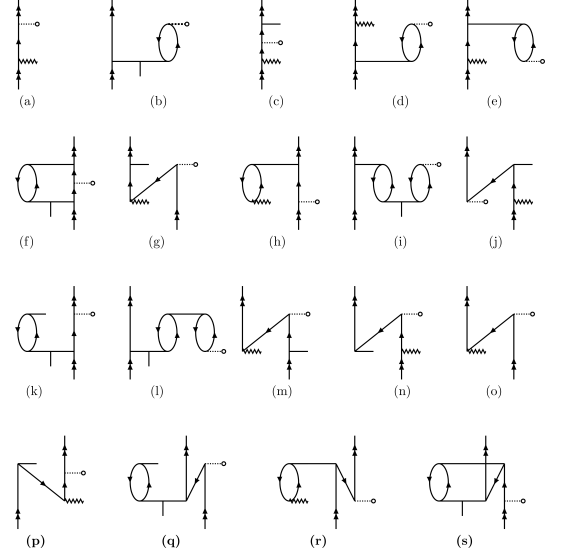


FIG. 7. Some example Goldstone diagrams contributing to $E1_{\text{elec}}^{\text{PNC}}$ for one-valence systems in Eq. (19).

1. Coupling with nuclear spin

As discussed earlier, the PNC diagrams, shown in Fig. 7, are defined in the electronic subspace. However, to calculate $E1_{\text{PNC}}^{\text{NSD}}$ the nuclear spin part of the PNC operator must be coupled with the operators in the electronic sector. For this reason the $E1_{\text{PNC}}^{\text{NSD}}$ diagrams must include a vertex which operates on the nuclear spin states. This coupling with nuclear part is done using the angular momentum algebra by following the conventions described in Lindgren and Morrison [29].

To elaborate on this, we choose one of the simple diagrams shown in Fig. 7(a) as an example. It arises from the CC operator $\mathbf{S}_1^{(1)}$, and subsumes the Dirac-Fock and dominant core-polarization contributions. Together these contributions make it the most dominant diagram contributing to $E1_{\text{elec}}^{\text{NSD}}$. The angular momentum diagram which represents coupling with the nuclear spin is shown in Fig. 8. Here, j_v , j_w and j_p represent the total angular momenta of the single particle states. The line k_1 represents a rank one multipole operator denoting the angular part of dipole operator. Similarly, k_2 is another rank one multipole operator which connects the electronic and nuclear sectors. Since \mathbf{I} is a diagonal operator, k_2 does not

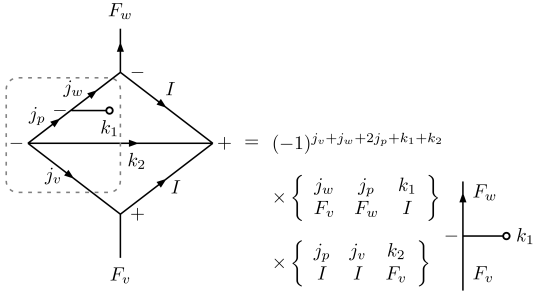


FIG. 8. Diagram showing the coupling of nuclear spin with electronic state and resulting angular factor. Portion within the rectangular dash line represents the electronic part, whereas the remaining portion is due to the coupling of nuclear spin and electronic angular momenta.

change the nuclear spin, whereas in the electronic sector it facilitates a transition from j_v to j_p states. The electronic and nuclear angular momenta (j_v , \mathbf{I}) and (j_w , \mathbf{I}) are coupled to give hyperfine states $|F_v\rangle$ and $|F_w\rangle$, respectively. Using the Wigner-Eckart theorem, we can write the algebraic expression for the coupled diagram, shown in Fig. 8, as

$$\begin{aligned} \langle F_w m_w | \mathbf{DS}_1^{(1)} \cdot \mathbf{I} | F_v m_v \rangle &= (-1)^{F_w - m_w} \\ &\times \begin{pmatrix} F_w & 1 & F_v \\ -m_w & q & m_v \end{pmatrix} \langle F_w || \mathbf{D}_{\text{eff}} || F_v \rangle. \end{aligned} \quad (21)$$

Here, $\mathbf{D}_{\text{eff}} = \mathbf{D}(\mathbf{S}_1^{(1)} \cdot \mathbf{I})$ is a rank one operator, m_i represents the hyperfine magnetic quantum number and q is the component of \mathbf{D}_{eff} . The phase factor and $3j$ -symbol correspond to the diagram on the right hand side of equation in Fig. 8.

III. RESULTS AND DISCUSSIONS

A. Single-particle basis and convergence of properties

Accurate single-electron basis is essential to get reliable results using FSRCC theory. In this work, we have used Gaussian-type orbitals (GTOs) [30] as the single-electron basis in all the calculations. The GTOs are expressed as a linear combination of the Gaussian-type functions (GTFs) and the GTFs used in defining the large component of the wavefunction are

$$g_{\kappa p}^L(r) = C_{\kappa i}^L r^{n_\kappa} e^{-\alpha_p r^2}. \quad (22)$$

Here, parameter $p = 0, 1, 2, \dots, N$ is the GTO index and N is the total number of GTFs. The exponent α_p is further expressed in terms of two independent parameters α_0 and β , as $\alpha_0 \beta^{p-1}$. Parameters α_0 and β are optimized separately for each orbital symmetry so that the single-electron wavefunctions and the corresponding energies match well with the numerical values obtained from GRASP2K [31]. To ensure a good quality basis, we have also compared our gaussian energies with B-spline energies [32]. The small components of

TABLE I. Orbital energies (in hartree) from GTO using Dirac-Coulomb Hamiltonian compared with GRASP2K [31] and B-Spline [32] results. The optimized α_0 and β parameters for even tempered GTO basis used in the calculations are also provided.

Orbitals	GRASP2K	B-spline	GTO
$1s_{1/2}$	1330.11688	1330.11804	1330.11562
$2s_{1/2}$	212.56408	212.56447	212.56407
$2p_{1/2}$	199.42926	199.42946	199.42939
$2p_{3/2}$	186.43638	186.43658	186.43658
$3s_{1/2}$	45.96965	45.96973	45.96966
$3p_{1/2}$	40.44825	40.44829	40.44828
$3p_{3/2}$	37.89430	37.89430	37.89431
$3d_{3/2}$	28.30949	28.30949	28.30950
$3d_{5/2}$	27.77517	27.77515	27.77516
$4s_{1/2}$	9.51283	9.51282	9.51280
$4p_{1/2}$	7.44630	7.44628	7.44628
$4p_{3/2}$	6.92101	6.92100	6.92100
$4d_{3/2}$	3.48563	3.48561	3.48562
$4d_{5/2}$	3.39691	3.39690	3.39690
$5s_{1/2}$	1.48981	1.48980	1.48980
$5p_{1/2}$	0.90789	0.90789	0.90789
$5p_{3/2}$	0.84033	0.84033	0.84033
E_{SCF}	7786.64263	7786.64638	7786.63884
Parameter	s	p	d
α_0	0.00340	0.00368	0.00495
β	1.779	1.766	1.829

wavefunctions are derived from the large components using the kinetic balance condition [33].

In Table I, we have provided the optimized single-electron and the self-consistent-field (SCF) energies for Cs and have compared them with GRASP2K and B-spline results. We have also tabulated the optimized values of the α_0 and β parameters. It is to be noted that, the single-electron basis used in the properties calculations incorporates the effects of vacuum polarization and the self-energy corrections. As evident from the table, the single-particle and SCF energies are in excellent agreement with the GRASP2K and B-spline results. The difference observed is of the order of *milli-hartree* or less.

Owing to the mathematically incomplete nature of GTOs, a check on the convergence of properties with basis size is essential to obtain reliable results using FSRCC. To assess the convergence of properties, in Tables IX and X of Appendix, we have listed the values of excitation energies, $E1$ matrix elements, HFS constants, and $E1_{\text{PNC}}^{\text{NSD}}$ as a function of increasing basis sizes. As discernible from the table, to obtain a converged basis set, we start with a moderate-size basis and add orbitals systematically to each symmetry until the change in the properties is less than or equal to 10^{-3} in the respective units. To visualize the trend, in Fig. 9, we show the convergence of excitation energies, HFS constants, and $E1$ matrix elements with the basis size. As discernible from the panel (a) of Fig. 9, all the properties converge well with the basis size. For an example, the change in the excitation energies is almost zero when the basis is augmented beyond 163 (19s, 17p, 16d, 15f, 13g, 11h) orbitals. So, we consider this as the optimized basis set and use it in the calculations by adding the

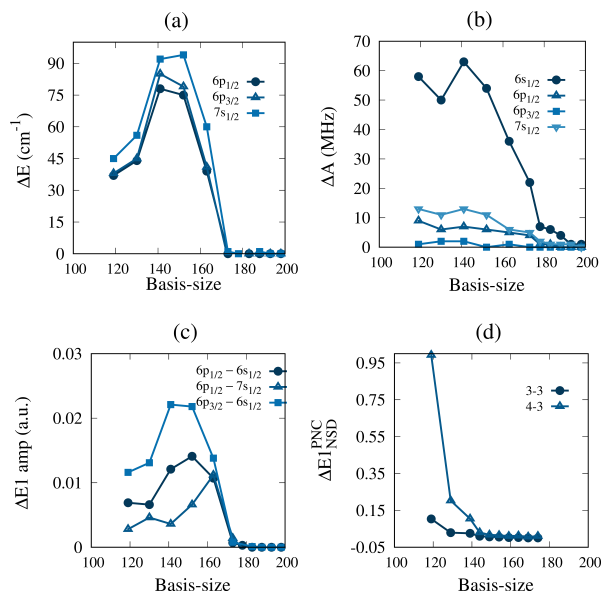


FIG. 9. Convergence of the properties results computed using FS-RCC theory with basis size.

TABLE II. Excitation energies (cm^{-1}) of some low lying states of Cs.

States	DC-CCSD	Breit	QED	Total	NIST [34]	% diff.
$6p_{1/2}$	11168	10	8	11186	11178	0.07
$6p_{3/2}$	11746	11	8	11765	11732	0.28
$7s_{1/2}$	18503	12	10	18535	18535	0.00
$7p_{1/2}$	21732	13	10	21755	21765	0.04
$7p_{3/2}$	21920	14	12	21946	21946	0.00

corrections from relativistic and QED effects.

B. Excitation energies, hyperfine structure constants and E1 transition amplitudes

In this section we present and discuss the excitation energies, MHFS constants, and the $E1$ transition amplitudes obtained from our computations. The excitation energies of a few low lying states of Cs from our computations are listed in Table II. To improve the accuracy of the excited energies, we have incorporated Breit interaction, self-energy and vacuum polarization corrections. The combined corrections from self-energy and vacuum polarization are listed as QED contribution. It is to be noted that, obtaining accurate energies indicates accuracy of the wavefunctions, which are used later to compute various properties. As evident from the table, the computed excitation energies are in excellent agreement with the NIST data [34]. Among the excited states, the $6p_{3/2}$ state has the largest deviation, our result is $\approx 0.3\%$ larger than the NIST data. It is, however, to be noted that the deviations of the excited states $6p_{1/2}$, $7s_{1/2}$, and $7p_{1/2}$, which have dominant contributions to the PNC matrix elements, are less than 0.1% . To be specific, our result of $6p_{1/2}$ excitation energy is

$\approx 0.07\%$ larger, whereas excitation energy of $7s_{1/2}$ is identical with the NIST data. Considering the contributions from the Breit and QED corrections, the contributions are at the maximum ≈ 0.09 and 0.07% , respectively, which occurs in the case of $6p_{1/2}$ state.

We now discuss and analyze our results of magnetic HFS (MHFS) constants listed in Table III. Since $H_{\text{PNC}}^{\text{NSD}}$ depends on the nuclear density, the wavefunction should be accurate within the nuclear region to obtain reliable value of $E1_{\text{PNC}}^{\text{NSD}}$. Similarly, considering that MHFS operator has a Dirac-delta function, the wave function should be accurate within the nuclear region to obtain accurate MHFS constants. Thus, MHFS constants obtained from theoretical calculations serve as an important measure to indicate the accuracy of wavefunctions in the small r region. For Cs there are several results of MHFS constants from previous works as it is a theoretically and experimentally well studied system. Our results along with those from the previous works are listed in Table III. Like in the case of excitation energies, to study the nature of electron correlations, we have provided the Breit and QED contributions separately. As evident from the table, for all the states our results for A are in good agreement with the experimental values.

For the $6s_{1/2}$ state, our result of 2308 MHz is in good agreement with the experimental value 2298.2 MHz. The deviation of $\approx 0.5\%$ is a trend common with the previous calculations. Among the theoretical results the smallest and largest deviations from experimental data are $\approx 0.2\%$ [8] and $\approx 0.8\%$ [35], respectively. Compare to other theoretical results, ours is on the higher side. One reason for this could be the inclusion of the corrections from the Breit and QED interactions. Without these our result of 2297.96 MHz is in better agreement with the experimental value of 2298.2 MHz.

In the case of $6p_{1/2}$, our result of 287.8 MHz is lower than the experimental as well as other theoretical results. The deviation from the average experimental value of 291.9 MHz is $\approx 1.4\%$. The contribution from the Breit interaction is more than an order magnitude larger than the QED correction and opposite in phase. As a result the Breit interaction reduces the value of A . From the table it is evident that our result without the Breit and QED corrections is closer to the experimental result. It is $\approx 0.7\%$ lower than the experimental data. An important observation is, there is a variation among the previous theoretical results. The difference between the lowest and highest values is $\approx 1.5\%$. There is limited data for the $6p_{3/2}$ state. There are only two results each from the previous theoretical and experimental studies for comparison. Our result of 49.79 MHz lies between the two experimental results, however, closer to the latest experimental result [43] with deviation of $\approx 0.9\%$. Our computed value is in good agreement with the previous two theoretical results.

Considering the state $7s_{1/2}$, there are several theoretical and experimental results from previous studies. Our result of 545.2 MHz is in excellent agreement with these data. It is $\approx 0.1\%$ larger than the average experimental value of 545.9 MHz. Again for the $7p_{1/2}$ state, there are several theoretical results from previous studies, however, there are only two experimental results. Most of the previous theoretical results are obtained using similar methods and have reported the simi-

TABLE III. Magnetic dipole hyperfine structure constants (MHz) for some low lying states and E1 transition amplitudes (a.u.) for allowed transitions in Cesium. The data from experiments and other theory calculations are also provided for comparison.

States/Transition	DC-CCSD	Breit	QED	Total	Other cal.	Exp.
MHFS (A)						
$6s_{1/2}$	2297.96	6.08	4.82	2308.86	2280.6 ^a , 2306(10) ^b , 2306.6 ^c , 2302 ^d 2300.3 ^e , 2291 ^f , 2293.3 ^g	2298.16 ^h , 2298.2 ^m
$6p_{1/2}$	289.77	-2.00	0.05	287.82	291 ^b , 291.49 ^c , 293.5 ^d 290.5 ^e , 292.7 ^f , 294.96 ^g	291.929(1) ^l , 291.91 ^o , 295.02 ⁱ
$6p_{3/2}$	51.01	-1.24	0.02	49.79	51.2 ^d , 49.8 ^f	47.19 ⁱ , 50.29 ^k
$7s_{1/2}$	544.44	-0.31	1.08	545.21	547 ^b , 544.59 ^c , 546.8 ^d 543.8 ^e , 544.0 ^f , 545.67(40) ^g	545.87(1) ^p , 545.82 ^q , 545.9 ^r 568.42 ⁱ , 546.3 ^h
$7p_{1/2}$	93.61	-0.59	0.01	93.03	94(1) ^b , 94.07 ^c , 94.0 ^d , 94.1 ^e , 94.21 ^f , 94.49(26) ^g	94.40(5) ^j , 94.35(4) ^s
$7p_{3/2}$	16.81	-0.38	0.01	16.44	17.1 ^d , 16.255 ^f	16.605(6) ^j
E1 amplitudes						
$6p_{1/2} \rightarrow 6s_{1/2}$	4.5378	0.0	-0.0006	4.5372	4.5487 ^y , 4.5093 ^c , 4.5052 ^z , 4.528 ^a	4.5010 ^v , 4.508 ^κ , 4.510 ^λ
$7p_{1/2} \rightarrow 6s_{1/2}$	0.2902	0.0	0.0003	0.2905	0.2769 ^c , 0.3006 ^y , 0.2776 ^z	0.2781(45) ^θ
$6p_{3/2} \rightarrow 6s_{1/2}$	6.4036	0.0	-0.0007	6.4029	6.3402 ^z	6.345 ^κ , 6.347 ^λ , 6.3349(48) ^ν
$7p_{3/2} \rightarrow 6s_{1/2}$	0.6075	-0.0001	-0.0001	0.6073	0.5741 ^z	0.5742(57) ^θ
$6p_{1/2} \rightarrow 7s_{1/2}$	4.2601	0.0	0.0007	4.2608	4.2500 ^y , 4.239 ^z , 4.245 ^c , 4.243 ^c	4.249(4) ^ζ
$7p_{1/2} \rightarrow 7s_{1/2}$	10.3165	-0.0001	-0.0011	10.3153	10.297 ^y , 10.297 ^z , 10.307 ^c	10.308(15) ^ζ
$6p_{3/2} \rightarrow 7s_{1/2}$	6.5189	0.0	0.0009	6.5198	6.507 ^β , 6.474 ^z , 6.480 ^c	6.489 ^ζ
$7p_{3/2} \rightarrow 7s_{1/2}$	14.3267	-0.0001	-0.0017	14.3249	14.303 ^z	

^a Ref. [35] - CC, ^b Ref. [36] - RCC, ^c Ref. [6] - CCSDvT, ^d Ref. [8] - MBPT, ^e Ref. [37] - All-order, ^f Ref. [38] - LRCC, ^g Ref. [39] - All-order CP, ^h Ref. [40] - Exp., ⁱ Ref. [41] - Exp., ^j Ref. [42] - Exp., ^k Ref. [43] - Exp., ^l Ref. [44] - Exp., ^m Ref. [45] - Exp., ⁿ Ref. [46] - Exp., ^o Ref. [47] - Exp., ^p Ref. [48] - Exp., ^q Ref. [49] - RCCSD, ^r Ref. [50] - AMPSCI, ^s Ref. [51] - Relati. HF, ^t Ref. [52] - Relati. All-order, ^u Ref. [53] - Exp., ^v Ref. [54] - Exp., ^w Ref. [55] - Exp., ^x Ref. [56] - Exp., ^y Ref. [57] - Exp.,

lar values. Our result of 93.0 MHz, is $\approx 1.3\%$ smaller than the experimental result. However, like in the results of other states, our result without Breit and QED corrections is closer to the experimental value. Lastly, for $7p_{3/2}$ state, our result of 16.4 MHz is in good agreement with the experimental value and is $\approx 0.9\%$ lower. Our result also matches well with the previous coupled-cluster result [38].

The E1 transition amplitudes from our calculations, along with the data from previous theoretical and experiment studies, are listed in the lower rows of Table III. In contrast to MHFS constants, the results of E1 is a test for the accuracy of wavefunctions in large r regions [50]. For the E1 amplitudes, there are several results from previous studies, and hence, a detailed comparison with each of the results is beyond the scope of the present work. However, as evident from the table, our results are in good agreement with the previous theory as well as experimental values listed in the table. In general, our results are closer to those reported in Refs. [6, 35, 49]. This could be attributed to the similar CC based methods employed in these works. The small deviations from the previous results could be due to the inclusion of corrections arising from the Breit and QED interactions, and the use of larger basis set in our calculations.

C. Electric dipole polarizability

In this section we discuss our results of α for the ground state $6s_{1/2}$, and excited states $6p_{1/2}$, $7s_{1/2}$ and $7p_{1/2}$. These

states are chosen as these are expected to contribute dominantly to $E1_{\text{PNC}}^{\text{NSD}}$ through the strong PNC and dipole induced mixings. It is to be noted that, α of an atom or ion is an important property relevant to several experiments to probe fundamental physics and technological applications. This is applicable to the present work as well. In particular, the computation of α involves the calculation of dipole matrix elements, which also contribute to $E1_{\text{PNC}}^{\text{NSD}}$. To compute α , we adopt two different methods. First, we employ the sum-over-states approach, where we use E1 matrix elements obtained from our computations, and the experimental energies to calculate α for $6s_{1/2}$, $6p_{1/2}$, $7s_{1/2}$ and $7p_{1/2}$ states. The values of α from this approach shall serve as a benchmark to gauge the accuracy of unperturbed wavefunctions and E1 transition amplitudes. And, second we use the FS-PRCC method, discussed earlier in the context of PNC perturbation, to compute α for $6s_{1/2}$ and $7s_{1/2}$ states. The values of α from this shall serve as an indicator of accuracy for the initial and final PNC perturbed states $\tilde{6}s_{1/2}$ and $\tilde{7}s_{1/2}$. Since the Goldstone diagrams for the polarizability are topologically same as PNC diagrams in the electronic sector, obtaining accurate value of α using FS-PRCC shall lead to accurate value of $E1_{\text{PNC}}^{\text{NSD}}$.

In the Tables IV and V, we have listed our results of α computed using sum-over states approach for $6s_{1/2}$, $6p_{1/2}$ and $7s_{1/2}$, $7p_{1/2}$ states, respectively. For comparison, we have also listed the results from other theoretical and experimental works. To assess the trend of electron correlations, contributions from the dominant E1 matrix elements are listed separately. For $6s_{1/2}$ state, as can be expected, the dominant con-

TABLE IV. Electric dipole polarizability (a.u.) of $6s_{1/2}$ and $6p_{1/2}$ states of Cs using sum-over-states approach. The dominant contributing E1 matrix elements are provided to quantify the nature of electron correlations.

Contr./E1 matrix	$\alpha_{6s_{1/2}}$
$6p_{3/2} \rightarrow 6s_{1/2}$	255.73
$6p_{1/2} \rightarrow 6s_{1/2}$	134.77
$7p_{3/2} \rightarrow 6s_{1/2}$	1.23
$7p_{1/2} \rightarrow 6s_{1/2}$	0.28
$8p_{3/2} \rightarrow 6s_{1/2}$	0.22
Core	15.8
Total	408.03
Others	$396.02^a, 399.9(1.9)^b, 401.0(6)^c$ $401.5^d, 398.4(19)^e$ $402(8)^f, 401.0(6)^g$
Exp.	$402(8)^f, 401.0(6)^g$
Contr./E1 matrix	$\alpha_{6p_{1/2}}$
$5d_{3/2} \rightarrow 6p_{1/2}$	1215.98
$7s_{1/2} \rightarrow 6p_{1/2}$	180.56
$6s_{1/2} \rightarrow 6p_{1/2}$	-134.76
$6d_{3/2} \rightarrow 6p_{1/2}$	89.45
$7d_{3/2} \rightarrow 6p_{1/2}$	34.39
$8d_{3/2} \rightarrow 6p_{1/2}$	21.45
$8s_{1/2} \rightarrow 6p_{1/2}$	6.62
$9d_{3/2} \rightarrow 6p_{1/2}$	6.54
$9s_{1/2} \rightarrow 6p_{1/2}$	3.64
$10s_{1/2} \rightarrow 6p_{1/2}$	1.70
$11s_{1/2} \rightarrow 6p_{1/2}$	0.50
Core	15.8
Total	1441.87
Other cal.	$1338(5.4)^e, 1404(28)^h, 1327^i$
Exp.	$1371^j, 1328.35^k$

^a Ref. [58] - RCCSDT, ^b Ref. [23] - RCCSD, ^c Ref. [59] - sum-over-states, ^d Ref. [60] - RLCCSD, ^e Ref. [61]- RLCCSDT, ^f Ref. [62] - Exp., ^g Ref. [56] - Exp., ^h Ref. [63] - sum-over-states, ⁱ Ref. [64] - RHF, ^j Ref. [65] - Exp., ^k Ref. [66] - Exp.

tribution comes from the dipole mixing with $6p_{1/2}$ and $6p_{3/2}$ states. As discernible from Fig. 10, they contribute $\approx 33\%$ and 63% , respectively, to the total value. Contribution from the core polarization, $\approx 4\%$, is the next leading order contribution. Comparing with the results from previous works, our value is larger than the other theoretical and experimental results. Our value of 408.03 is $\approx 1.7\%$ larger than the recent experiment [56]. The reason for this could be attributed to larger values of $6s_{1/2} \rightarrow 6p_{1/2}$ and $6s_{1/2} \rightarrow 6p_{3/2}$ matrix elements than experiment. Contributions from the intermediate states with $n \geq 8$ are found to be small.

For the $6p_{1/2}$ state, the dominant contribution of $\approx 84\%$ arises from the dipole mixing with $5d_{3/2}$ state. The next two dominant contributions are from the $7s_{1/2}$ and $6s_{1/2}$ states. These contribute $\approx 12\%$ and -9% , respectively. The other two significant contributions are from the $6d_{3/2}$ and $7d_{3/2}$ states contributing $\approx 6\%$ and 2% , respectively. Comparing with the previous theoretical works, there is a spread in the reported values. The result from the relativistic Hartree-Fock method in Ref. [64] is $\approx 6\%$ smaller than the sum-over-states value in Ref. [63]. A similar trend is also there among the ex-

TABLE V. Electric dipole polarizability (a.u.) of $7s_{1/2}$ and $7p_{1/2}$ states of Cs using sum-over-states approach. The dominant contributing E1 matrix elements are provided to quantify the nature of electron correlations.

Contr./E1 matrix	$\alpha_{7s_{1/2}}$
$7p_{3/2} \rightarrow 7s_{1/2}$	4417.09
$7p_{1/2} \rightarrow 7s_{1/2}$	2414.83
$6p_{3/2} \rightarrow 7s_{1/2}$	-451.13
$6p_{1/2} \rightarrow 7s_{1/2}$	-180.56
$8p_{3/2} \rightarrow 7s_{1/2}$	33.50
$8p_{1/2} \rightarrow 7s_{1/2}$	10.25
$9p_{3/2} \rightarrow 7s_{1/2}$	2.50
$9p_{1/2} \rightarrow 7s_{1/2}$	0.35
$10p_{1/2} \rightarrow 7s_{1/2}$	0.01
$10p_{3/2} \rightarrow 7s_{1/2}$	0.00
Core	15.8
Total	6256.64
Other cal.	$6238^a, 6061^b, 6140^c$
Exp.	6238^d
Contr./E1 matrix	$\alpha_{7p_{1/2}}$
$6d_{3/2} \rightarrow 7p_{1/2}$	29919.87
$8s_{1/2} \rightarrow 7p_{1/2}$	2570.51
$7s_{1/2} \rightarrow 7p_{1/2}$	-2413.06
$7d_{3/2} \rightarrow 7p_{1/2}$	890.96
$8d_{3/2} \rightarrow 7p_{1/2}$	83.87
$5d_{3/2} \rightarrow 7p_{1/2}$	-65.39
$9s_{1/2} \rightarrow 7p_{1/2}$	52.75
$9d_{3/2} \rightarrow 7p_{1/2}$	22.26
$10s_{1/2} \rightarrow 7p_{1/2}$	6.72
Core	15.8
Total	31084.29
Other cal.	$29900(700)^a$
Exp.	$29600(600)^e$

^a Ref. [61]- RLCCSDT, ^b Ref. [64] - RHF, ^c Ref. [67] - sum-over-states., ^d Derived from the experiments Refs. [68] and [56], ^e Ref. [69] - Exp.

perimental values. Our result is closer to the sum-over-states value [63].

For the $7s_{1/2}$ state, two states $7p_{1/2}$ and $7p_{3/2}$ contribute dominantly to α , their combined result 6831.92 a.u. is larger than the net value 6256.64 a.u. The reason is, the contributions from both the next two dominant states $6p_{1/2}$ and $6p_{3/2}$ are in opposite phase. These two states together has a contribution of -631.69 a.u. The contributions from the remaining intermediate states $np_{1/2}$ and $np_{3/2}$ continue to decrease with higher n . We incorporate upto $n = 10$ and contribution from $10p_{3/2}$ is negligible and hence, contributions from $n > 10$ can be neglected. Our net value, 6256.64 a.u. is in good agreement with the experimental value, 6238 a.u. Considering the previous calculations, there are large differences among the reported values, 6061 [64], 6140 [67] and 6238 [61]. Our result is on the higher side of these and closer to Ref. [61]. For the α of $7p_{1/2}$, state $6d_{3/2}$ has the leading contribution $\approx 96\%$. The next leading contributions, almost equal in magnitude but opposite in phase, arise from the $7s_{1/2}$ and $8s_{1/2}$ states. These states together contribute $\approx 8\%$. Like the trends

TABLE VI. Electric dipole polarizability (a.u.) of the ground state, $6s_{1/2}$, and excited state $7s_{1/2}$ of Cs using FS-PRCC theory. For quantifying electron correlations embedded in FS-PRCC, the termwise contributions are listed separately.

Term + H. c.	$6s_{1/2}$	$7s_{1/2}$
Dirac-Fock	647.257	8060.598
$\mathbf{DS}_1^{(1)}$	-188.874	-1423.122
$\mathbf{DS}_2^{(1)}$	-14.867	-35.864
$S_1^{(0)\dagger} \mathbf{DS}_1^{(1)}$	-23.789	-338.479
$S_2^{(0)\dagger} \mathbf{DS}_1^{(1)}$	-13.816	-29.974
$S_2^{(0)\dagger} \mathbf{DS}_2^{(1)}$	-0.702	-1.641
$\mathbf{DT}^{(1)}$	-0.722	-0.120
$T^{(0)\dagger} \mathbf{DT}^{(1)}$	-0.002	0.001
$T^{(0)\dagger} \mathbf{DS}^{(1)}$	1.929	4.818
$S^{(0)\dagger} \mathbf{DT}^{(1)}$	-1.570	-0.649
Normalization	-4.773	-11.437
Total PRCC	400.071	6224.131
PRCC + Breit	400.107	6224.691
PRCC + Breit + QED	399.895	6221.392
PRCC + Breit + QED + Triples	399.901	6221.423
Recommended	399.90 ± 4.0	6221.42 ± 62.2

of other states, our sum-over-states results are higher than the previous theoretical results. It should, however, be noted that, the $E1$ matrix elements used in the calculations of α are all from our FSRCC calculations, which is *ab initio*.

In the Table VI, we have listed the FS-PRCC results of α for initial and final PNC-perturbed states, $6s_{1/2}$ and $7s_{1/2}$. These computations are done using a basis set of moderate size ($11s, 10p, 8d, 10f, 8g, 8h$). To improve the results further, corrections from the Breit, QED and perturbative triples are also included. As it is evident from the table, our PRCC results of 399.90 a.u. and 6221.42 a.u. for the $6s_{1/2}$ and $7s_{1/2}$ states, respectively, are in excellent agreement with the experimental results 401 a.u. [56] and 6238 a.u. [56, 68], with a small deviation of $\approx 0.3\%$ in each case. The reason for such a good match could be attributed to the merits of the FS-PRCC theory to incorporate the effect of external perturbation in many-body calculations. In contrast to the sum-over-states approach, the FS-PRCC theory subsumes the effects of all intermediate states implicitly through the PRCC operator.

Examining the termwise contributions, as expected, in both the states the dominant contribution arises from the Dirac-Fock (DF). The next leading order contribution is from $\mathbf{DS}_1^{(1)}$ + H.c, however it is opposite in phase to the dominant term. So, there is a significant cancellation between the two important contributions. A large contribution from this term is expected as $\mathbf{DS}_1^{(1)}$ subsumes the dominant contributions from core polarization and *valence-virtual* correlation effects. The next two leading order terms are $S_1^{(0)\dagger} \mathbf{DS}_1^{(1)}$ + H.c. and $\mathbf{DS}_2^{(1)}$ + H.c. They contribute $\approx -6(-6)\%$ and $-4(0.6)\%$, respectively, for $6s_{1/2}(7s_{1/2})$ state. Further, the terms $S_2^{(0)\dagger} \mathbf{DS}_1^{(1)}$ + H.c., which are second order in cluster operators, have contributions of similar order to $\mathbf{DS}_2^{(1)}$. Other

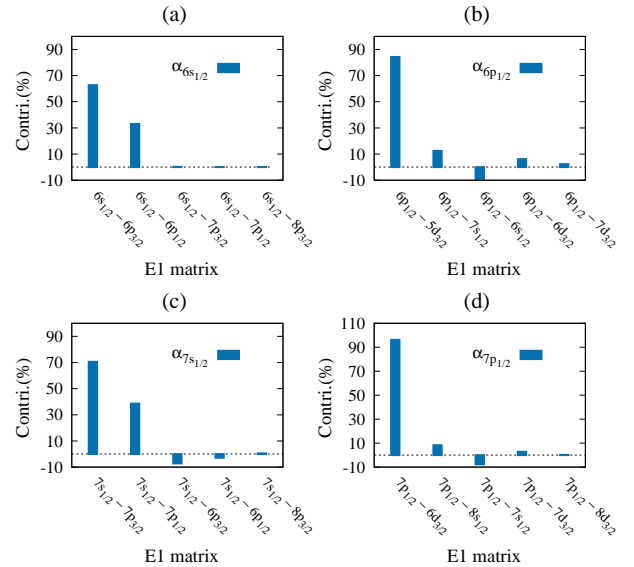


FIG. 10. Five dominant contributing dipolar mixings to α for $6s_{1/2}$, $6p_{1/2}$, $7s_{1/2}$, and $7p_{1/2}$ states.

terms with two orders of CC operators have small contributions.

D. NSD-PNC amplitudes

In this section we present and discuss the results of $E1_{\text{PNC}}^{\text{NSD}}$, which are listed in Table VII for transitions between different hyperfine states. To quantify the importance of electron correlations, in the table we have listed results from different methods with increasing sophistication. Thus, among the methods, DF listed as first does not include any electron-correlation and the last, PRCC(T)+Bre.+QED is the one which includes maximum electron-correlation effects among all the methods. As expected, the dominant contribution to $E1_{\text{PNC}}^{\text{NSD}}$ is from the DF for all the hyperfine transitions. It contributes $\approx 91\%$, 87% , 84% and 91% of the PRCC value for the $3 \rightarrow 3$, $3 \rightarrow 4$, $4 \rightarrow 3$ and $4 \rightarrow 4$ hyperfine transitions, respectively. The next leading order contribution is from the first-order MBPT, where contribution of $\approx -13.5\%$ is observed for both $3 \rightarrow 3$ and $4 \rightarrow 4$ transitions. Whereas, there are in-phase contributions of $\approx 16.5\%$ and 12.2% for $3 \rightarrow 4$ and $4 \rightarrow 3$ transitions, respectively. Similarly, the second and third-order MBPT also show a mix trend of opposite and in-phase contributions, however, with smaller magnitudes. Among the four transitions the contribution from MBPT(2) is larger ($\approx -2\%$) in the case of $3 \rightarrow 4$ and $4 \rightarrow 3$. And, MBPT(3) is, however, has a more prominent contribution of $\approx 3\%$ in the case of $3 \rightarrow 3$ and $4 \rightarrow 4$ transitions.

Among the previous theoretical works, we could find two published works which reported the values of $E1_{\text{PNC}}^{\text{NSD}}$ for all the four transitions. The first one is by Johnson and collaborators using RPA [12], and second is by Safronova and collaborators [13] using the all-order method. For $3 \rightarrow 3$ and $4 \rightarrow 4$

TABLE VII. The $E1_{\text{PNC}}^{\text{NSD}}$ of $6s_{1/2} \rightarrow 7s_{1/2}$ transition in units of $iea_0 \times 10^{-12} \mu'_W$. To assess the nature of electron correlations, contributions from different levels of the theory used is provided separately. For comparison, the data available from other theory calculations are also provided.

Methods	Transition $F_v \rightarrow F_w$			
	3 \rightarrow 3	3 \rightarrow 4	4 \rightarrow 3	4 \rightarrow 4
DF	1.821	4.729	5.430	2.073
MBPT(1)	1.551	5.624	6.220	1.766
MBPT(2)	1.570	5.492	6.097	1.788
MBPT(3)	1.636	5.490	6.120	1.863
PRCC	1.997	5.419	6.452	2.273
PRCC(T)	1.998	5.420	6.453	2.273
PRCC(T)+Bre.	1.993	5.406	6.368	2.268
PRCC(T)+Bre. + QED	2.000	5.425	6.250	2.276
Reco.	2.00 \pm 0.02	5.43 \pm 0.05	6.25 \pm 0.06	2.28 \pm 0.02
Other cal	2.249 ^a	6.432 ^a	7.299 ^a	2.560 ^a
	2.274 ^c	7.948 ^b	7.057 ^b	2.589 ^c
	2.334 ^d	5.446 ^c , 6.496 ^d	6.313 ^c , 7.394 ^d	2.658 ^d

^a Ref. [12], ^b Ref. [13] ^c Ref. [14] ^d Ref. [15]

TABLE VIII. Termwise contributions to $E1_{\text{PNC}}^{\text{NSD}}$. Values listed are in the unit of $iea_0 \times 10^{-12} \mu'_W$

Term + H. c.	3 \rightarrow 3	3 \rightarrow 4	4 \rightarrow 3	4 \rightarrow 4
$\mathbf{DS}_1^{(1)}$	3.3696	6.3157	7.9280	3.8634
$\mathbf{DS}_2^{(1)}$	-0.0643	-0.3453	-0.4078	-0.0732
$S_1^{(0)\dagger} \mathbf{DS}_1^{(1)}$	-1.0649	-0.3784	-0.7988	-1.2124
$S_2^{(0)\dagger} \mathbf{DS}_1^{(1)}$	-0.0653	0.1455	0.1288	-0.0744
$S_2^{(0)\dagger} \mathbf{DS}_2^{(1)}$	-0.0023	-0.0271	-0.0337	-0.0027
$\mathbf{DT}^{(1)}$	-0.0993	-0.1936	-0.2318	-0.1130
$T_1^{(0)\dagger} \mathbf{DT}_1^{(1)}$	0.0000	-0.0028	-0.0028	0.0000
$T_2^{(0)\dagger} \mathbf{DT}_1^{(1)}$	-0.0131	0.0074	0.0024	-0.0149
$S_1^{(0)\dagger} \mathbf{DT}_1^{(1)}$	-0.0083	0.0273	0.0241	-0.0094
$S_2^{(0)\dagger} \mathbf{DT}_1^{(1)}$	-0.0132	-0.0213	-0.0264	-0.0150
$T_2^{(0)\dagger} \mathbf{DT}_2^{(1)}$	-0.0031	-0.0020	-0.0032	-0.0035
Normalization	-0.0392	-0.1063	-0.1266	-0.0446
Total	1.9966	5.4190	6.4521	2.2732

transitions, our results of 2.0×10^{-12} and 2.28×10^{-12} , respectively, are lower than the RPA results. The reason for this may be attributed to improved consideration of electron correlations in our work. In our computations, the residual Coulomb interaction is incorporated to all orders of perturbation using relativistic FSRCC theory. Similarly, the PNC interaction is treated using the FS-PRCC theory. As discussed earlier, in contrast to the sum-over-states approach, PRCC includes contributions from all the possible intermediate states in the calculation of $E1_{\text{PNC}}^{\text{NSD}}$.

For the 3 \rightarrow 4 and 4 \rightarrow 3 transitions, there is a large difference between the previous results. For example, the all-order value [13] for 3 \rightarrow 4 transition is $\approx 20\%$ higher than

the RPA value [12]. This implies that the electron correlation effects must be treated accurately to get reliable values of $E1_{\text{PNC}}^{\text{NSD}}$. Our results are lower than both the previous results. It is, however, to be noted that our DF results of 1.82×10^{-12} , 4.73×10^{-12} , 5.43×10^{-12} and 2.07×10^{-12} , for 3 \rightarrow 3, 3 \rightarrow 4, 4 \rightarrow 3 and 4 \rightarrow 4 transitions, respectively, are in good agreement with the values reported in Ref. [12]. Thus, the difference from the previous works [12, 13] is due to better consideration of electron correlations in our work.

Apart from Refs. [12, 13], there are two previous works [14, 15] which report results on $E1_{\text{PNC}}^{\text{NSD}}$ for considered hyperfine transitions. Both of the works use CC method like the present work, however, with some key differences. There is a slight difference in the $E1_{\text{PNC}}^{\text{NSD}}$ values with respect to Ref. [14] for all the hyperfine transitions. This could be attributed to improved consideration of electron correlation effects due to the inclusion of nonlinear terms of the PRCC theory in the present work. Whereas Ref. [14] is based on *linearized* PRCC theory. Our results of $E1_{\text{PNC}}^{\text{NSD}}$ are lower than Ref. [15] for all hyperfine transitions. One possible reason for this could be the incorporation of the corrections from Breit interaction, QED effects and perturbative triples. These were not considered in the previous works. Thus, the present work includes important many-body effects not included in the previous theoretical studies of NSD-PNC of Cs.

The Table VIII lists the term wise contribution to $E1_{\text{PNC}}^{\text{NSD}}$. As seen from the table, for all the hyperfine transitions, the leading order (LO) contribution is from the $\mathbf{DS}_1^{(1)} + \text{H.c.}$ term. This is natural, as it subsumes the contribution from DF, and the dominant contributions from *core-polarization* and *valence-virtual* correlation effects. It contributes ≈ 169 and 170% , of the total PNC amplitude, for 3 \rightarrow 3 and 4 \rightarrow 4 transitions, respectively. Whereas, the contribution is ≈ 117 and 123% for 3 \rightarrow 4 and 4 \rightarrow 3 transitions, respectively. The next leading order (NLO) term is $S_1^{(0)\dagger} \mathbf{DS}_1^{(1)} + \text{H.c.}$ It has an opposite contribution of $\approx -53\%$ for both the diagonal transitions. For off-diagonal transition 3 \rightarrow 4 and 4 \rightarrow 3, however, contributions vary, to ≈ -7 and -12% , respectively. Based on the LO and NLO contributions one can infer that the one-body perturbed cluster operator, $\mathbf{S}_1^{(1)}$, subsumes the dominant correlation effects from the PNC perturbation. For the next dominant contribution, the diagonal and off-diagonal hyperfine transitions show different trends of electron correlation effects. Interestingly, unlike in α , for 3 \rightarrow 3 and 4 \rightarrow 4 transitions, the next dominant contribution arise from the core electrons through the $\mathbf{DT}^{(1)} + \text{h. c.}$ terms. It contributes $\approx -5\%$ of the total amplitude. However, for the 3 \rightarrow 4 and 4 \rightarrow 3 transitions the term $\mathbf{DS}_2^{(1)} + \text{H.c.}$ provides the dominant contribution of $\approx -6\%$ for both the transitions.

E. PNC mixing, correlation effects, and other corrections

To examine the different many-body effects in finer detail, we consider and analyze the important terms. To begin with we take the PNC induced orbital mixing. This may be discernible from the orbital-wise contributions to the LO term

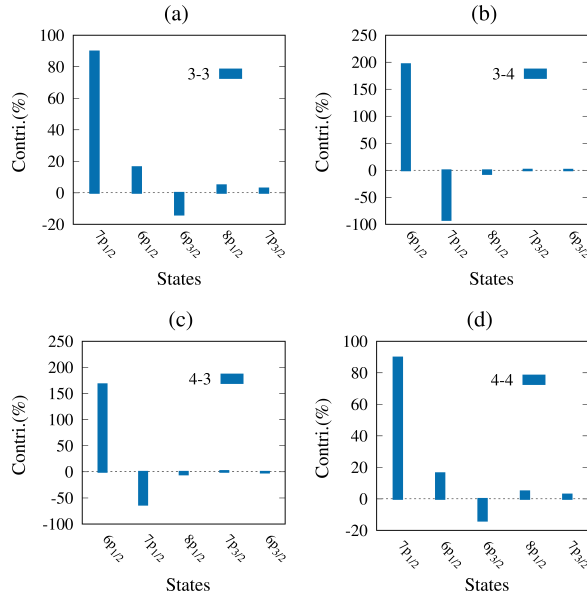


FIG. 11. Five dominant contributions from orbitals to $E1_{\text{PNC}}^{\text{NSD}}$. The percentage contribution is calculated with respect to the leading order term $\mathbf{DS}_1^{(1)}$.

$\mathbf{DS}_1^{(1)}$. As seen from Fig. 11, the $3 \rightarrow 3$ and $4 \rightarrow 4$ transitions have the same trend. In both, interestingly, the largest contribution $\approx 90\%$ of $\mathbf{DS}_1^{(1)}$ arises from the PNC induced mixing with $7p_{1/2}$ state. This is due to small energy difference with $7s_{1/2}$ state. The next dominant mixing is from the $6p$ state. In particular, $6p_{1/2}$ state has a contribution of $\approx 16\%$, whereas the $6p_{3/2}$ state has an opposite phase contribution of -14% . The next two significant contributions are from the $8p_{1/2}$ and $7p_{3/2}$ states, they contribute $\approx 5\%$ and 3% , respectively. The $3 \rightarrow 4$ and $4 \rightarrow 3$ transitions also have a similar trend. For both the transitions, the dominant PNC mixing is with the $6p_{1/2}$ state. Contributions of ≈ 196 and 167% to $\mathbf{DS}_1^{(1)}$ is observed for the $3 \rightarrow 4$ and $4 \rightarrow 3$ transitions, respectively. The next largest mixing with an opposite phase of $\approx -92\%$ and -63% , respectively, are there from the $7p_{1/2}$ state. The $8p_{1/2}$ and $7p_{3/2}$ are the next two dominant contributors. There is a contribution of $\approx -7(1.2)\%$ and $\approx -5(1.5)\%$ for the $3 \rightarrow 4$ and $4 \rightarrow 3$ transitions, respectively, from the $8p_{1/2}(7p_{3/2})$ state. The $6p_{3/2}$ state is the fifth dominant contribution with $\approx 1.0\%$ and -1.4% , respectively, to the two transitions. The other important contributions which merit closer study are the core-polarization effects, valence-virtual correlation, Breit and QED effects, and triple corrections. Each of these are addressed in detail.

1. Core polarization and valence-virtual correlation effects

To quantify the contributions from core polarization and valence-virtual correlation effects to $E1_{\text{PNC}}^{\text{NSD}}$, we again consider the LO term $\mathbf{DS}_1^{(1)}$. As discernible from the Goldstone

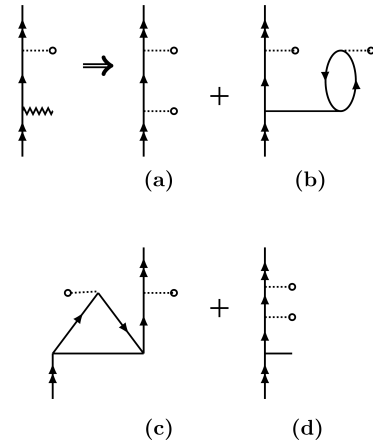


FIG. 12. The DF (diagram (a)), core-polarization (diagrams (b) and (c)) and valence-virtual (diagram (d)) contributions subsumed in the term $\mathbf{DS}_1^{(1)}$.

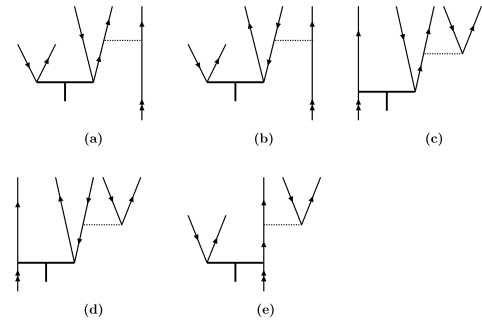


FIG. 13. Perturbative $\mathbf{S}_3^{(1)}$ diagrams arising from $g\mathbf{T}_2^{(1)}$ ((a) and (b)) and $g\mathbf{S}_2^{(1)}$ ((c), (d) and (e)) terms.

diagrams in Fig. 12, the term $\mathbf{DS}_1^{(1)}$ subsumes the contributions from DF, core-polarization (CP) and valence-virtual correlation (VC) effects. In particular, the diagrams Fig. 12(b) and 12(c) contribute to CP through dipole mixing between unperturbed states. The other dominant contribution to CP is from $\mathbf{S}_2^{(1)}$ through the term $\mathbf{DS}_2^{(1)}$. And, the corresponding diagrams are Fig. 7(b) and its exchange. An estimate of the VC correlation is obtained by subtracting the contributions of the first three diagrams in Fig. 12 from the $\mathbf{DS}_1^{(1)}$ value. In Fig. 14 we have shown the contributions from DF, CP and VC to the $3 \rightarrow 3$ and $4 \rightarrow 3$ hyperfine transitions. As discernible from Fig. 14 (c) and 14(d), as expected, DF has the largest contribution. It is $\approx 91\%$ and 84% of total value to $3 \rightarrow 3$ and $4 \rightarrow 3$ transitions, respectively. Considering the CP and VC contributions, they are in opposite phase for all the hyperfine transitions, and in terms of magnitude, VC has a larger contribution. For example, for $3 \rightarrow 3$ diagonal transition, VC contributes $\approx 111\%$ to the value of $\mathbf{DS}_1^{(1)}$, whereas the contribution from CP is $\approx -67\%$. A similar trend of contributions with $\approx 87\%$ and $\approx -67\%$, respectively, is also observed for the off-diagonal $4 \rightarrow 3$ transition.

2. Breit and QED interactions

In the Table VII we have listed the contributions from Breit and QED corrections to $E1_{\text{PNC}}^{\text{NSD}}$. The QED results are the combined contribution from vacuum polarization and the self-energy correction. To compute the correction from vacuum polarization, we use the Uehling potential [70] with a modification to incorporate the finite size nuclear charge distribution [71, 72],

$$V_{\text{Ue}}(r) = -\frac{2\alpha}{3r} \int_0^\infty dx x \rho(x) \int_1^\infty dt \sqrt{t^2 - 1} \left(\frac{1}{t^3} + \frac{1}{2t^5} \right) \times \left(e^{-2ct|r-x|} - e^{-2ct(r+x)} \right), \quad (23)$$

here, α is the fine structure constant, and should not be confused with dipole polarizability and $\rho(x)$ is the finite size Fermi density distribution of the nuclear charge. The corrections from the self-energy to single-electron energies are incorporated through the model Lamb-shift operator introduced by Shabaev *et al.* [73] and using the code QEDMOD [74]. Quantitatively, the contributions with respect to PRCC values are shown Fig.14(e) and Fig.14(f). We observe two important trends in the contributions from the Breit and QED corrections. First, both contribute with the same phase for off-diagonal transitions, whereas they have opposite contributions for diagonal transitions. Second, the contribution to the off-diagonal transition $4 \rightarrow 3$ is larger. In terms of magnitude, the largest cumulative contribution from Breit and QED corrections is $\approx 3.2\%$ of the PRCC value. This is significant and cannot be neglected.

3. Perturbative triples

To compute the contributions from perturbative triples to $E1_{\text{PNC}}^{\text{NSD}}$, we used our approach for polarizability of one-valence systems [21]. As discussed earlier, the PNC diagrams are topologically identical with the polarizability diagrams in the electronic sector. However, to obtain $E1_{\text{PNC}}^{\text{NSD}}$ we have to incorporate coupling with the nuclear spin. As the effect of external perturbation is included through the perturbed CC operators in PRCC theory, we pick the perturbative triples arising from $\mathbf{T}_2^{(1)}$ and $\mathbf{S}_2^{(1)}$. After contracting with the residual Coulomb interaction, $\bar{g}\mathbf{T}_2^{(1)}$ and $\bar{g}\mathbf{S}_2^{(1)}$, they lead to five $\mathbf{S}_3^{(1)}$ diagrams shown in Fig. 13. A dominant contribution to $E1_{\text{PNC}}^{\text{NSD}}$ is expected from the contraction of $\tilde{\mathbf{S}}_3^{(1)}$ with $S_2^{(0)}$ due to larger amplitudes of $S^{(0)}$ for one-valence systems. This leads to 49 Goldstone diagrams [21], which are first calculated in the electronic sector and then coupled with the nuclear spin. The contributions from perturbative triples to $E1_{\text{PNC}}^{\text{NSD}}$ amplitudes are listed in Table VII. Consistent with the trend in α , the contribution from triples to $E1_{\text{PNC}}^{\text{NSD}}$ is small. The largest contribution to $E1_{\text{PNC}}^{\text{NSD}}$ amplitudes is found to be $\approx 0.02\%$.

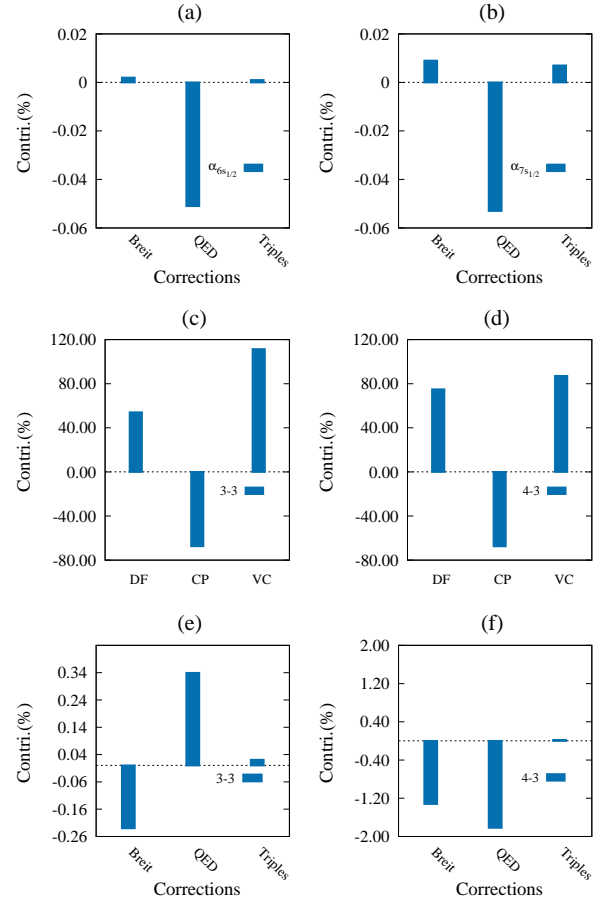


FIG. 14. The percentage contributions from Breit, QED and perturbative triples to α (panels (a), (b)) and $E1_{\text{PNC}}^{\text{NSD}}$ (panels (e), (f)). The percentage contributions from DF, CP and VC to $E1_{\text{PNC}}^{\text{NSD}}$ (panels (c), (d)).

IV. THEORETICAL UNCERTAINTY

Considering the approximations employed in the computation of $E1_{\text{PNC}}^{\text{NSD}}$, we identify four sources of theoretical uncertainties. The first one is the truncation of the orbital basis. From the convergence data of the $E1_{\text{PNC}}^{\text{NSD}}$ with basis size, for the basis up to h -symmetry, the change in $E1_{\text{PNC}}^{\text{NSD}}$ is $\approx 0.2\%$ when the optimal basis set with 169 orbitals is augmented. This is noticeable from the plots in (Fig. 9(d)). To estimate the uncertainty associated with the orbitals beyond h -symmetry we resort to the detailed analysis presented in Ref. [75], our previous work on α of one-valence atoms. Where we have shown that the largest overall contribution from the i, j and k symmetry orbitals to polarizability is $\approx 0.06\%$. Thus, the combined contribution from the orbitals of k and higher symmetries is expected to be smaller and we take 0.1% as an upper bound. So, the upper bound on the total uncertainty from the basis truncation is 0.3% . The second source of uncertainty is the truncation of the dressed operator $\bar{\mathbf{D}}$ to $\mathbf{D} + \mathbf{D}T^{(0)} + T^{(0)\dagger}\mathbf{D} + T^{(0)\dagger}\mathbf{D}T^{(0)}$. To estimate the uncertainty from this source, we again use the findings from our

previous work [25] where we showed that the combined contributions from terms with third-order in $T^{(0)}$ and higher is less than 0.1%. So, we take this as the upper bound from this source. The third source of uncertainty is the truncation of CC operators to singles and doubles. Among the higher excitations, triple excitations is the most prominent, and the dominant contribution is subsumed in the perturbative triples. So, to incorporate the dominant contribution from triple excitations, we have included the contributions from the perturbative triples arising from $S^{(0)\dagger}DgS_2^{(1)}$ and $S^{(0)\dagger}DgT_2^{(1)}$. The largest contribution from perturbative triples is observed to be $\approx 0.02\%$. Considering this we take 0.1% as an upper bound of the uncertainty due to the exclusion of contributions non-perturbative triples and higher excitations. The last source of theoretical uncertainty is associated with the frequency-dependent Breit interaction which is not included in our calculations. To estimate an upper bound of this source we use the results in our previous work [18], where using GRASP2K we estimated an upper bound of 0.13% for Ra. As Cs is lighter than Ra, the contribution is expected to be smaller. And, thus we take 0.13% as the uncertainty from this source. There could be other sources of theoretical uncertainties, such as the higher order coupled perturbation of vacuum polarization and self-energy terms, etc. These, however, have much smaller contributions and their combined uncertainty could be below 0.1%. Combining the upper bounds of all the four sources of uncertainties, we estimate a maximum theoretical uncertainty of 1% in the computed values of $E1_{\text{PNC}}^{\text{NSD}}$ amplitudes.

V. CONCLUSIONS

We have implemented a Fock-space perturbed relativistic coupled-cluster theory to compute the NSD-PNC transition amplitudes. Using the method we study the NSD-PNC of Cs atom. To check the wavefunctions obtained, we calculated the excitation energies for low lying states, E1 transition amplitudes, hyperfine structure constants, and dipole polarizability of the ground and low lying excited states. And, to improve the accuracy of the computed properties, the contributions from the Breit interaction and QED corrections are incorporated.

Our results of excitation energies, E1 transition amplitudes and hyperfine constants are in good agreement with the experimental data. Our results of α using sum-over-states approach

are marginally larger than the experimental results. This may be attributed to the fact that the sum-over-states approach does not include the contributions from all the intermediate states. As can be expected, our results using FS-PRCC are in excellent agreement with the experimental results. Our results of $E1_{\text{PNC}}^{\text{NSD}}$ are in general lower than the previous calculations. However, it should be noted that there is a variation among the previous results.

From the quantitative analysis of the electron correlations, we find that for the α of $6s_{1/2}$ and $7s_{1/2}$ states the dominant contribution is from the dipolar mixing with $6p$ and $7p$ states, respectively. For $6p_{1/2}$ and $7p_{1/2}$, however, the dominant dipolar mixing is observed with $5d_{3/2}$ and $6d_{3/2}$ states, respectively. Considering the $E1_{\text{PNC}}^{\text{NSD}}$, for both diagonal transitions $3 \rightarrow 3$ and $4 \rightarrow 4$, the first two dominant PNC mixings are from the $7p_{1/2}$ and $6p_{1/2}$ states. Similarly, both the off-diagonal transitions $3 \rightarrow 4$ and $4 \rightarrow 3$ are from the $6p_{1/2}$ and $7p_{1/2}$ states. Based on our results, the largest combined contribution from the Breit and QED corrections to $E1_{\text{PNC}}^{\text{NSD}}$ is $\approx 3.2\%$. Hence it is important to consider these corrections to obtain reliable value of $E1_{\text{PNC}}^{\text{NSD}}$.

ACKNOWLEDGMENTS

The authors wish to thank Palki Gakkhar for the useful discussions. Suraj Pandey acknowledges the funding support from the Ministry of Education, Govt. of India. BKM acknowledges the funding support from SERB, DST (CRG/2022/003845). The results presented in the paper are based on the computations using High Performance Computing clusters Padum and TEJAS at the Indian Institute of Technology Delhi, New Delhi.

Appendix A: Convergence of excitation energies, E1 amplitudes and MHFS constants

In Table IX, we show trend of the convergence of excitation energy, E1 transition amplitude, and magnetic dipole hyperfine structure constants as a function of the basis size. Similarly, the basis dependent results on $E1_{\text{PNC}}^{\text{NSD}}$ are provided in Table X. As it is evident from the table, all the properties converge to the order of 10^{-3} or less in the respective units of the properties.

-
- [1] B. M. Roberts, V. A. Dzuba, and V. V. Flambaum, "Parity and time-reversal violation in atomic systems," *Annual Review of Nuclear and Particle Science* **65**, 63–86 (2015).
- [2] M. S. Safronova, D. Budker, D. DeMille, Derek F. Jackson Kimball, A. Derevianko, and Charles W. Clark, "Search for new physics with atoms and molecules," *Rev. Mod. Phys.* **90**, 025008 (2018).
- [3] K. Tsigutkin, D. Dounas-Frazer, A. Family, J. E. Stalnaker, V. V. Yashchuk, and D. Budker, "Observation of a large atomic parity violation effect in ytterbium," *Phys. Rev. Lett.* **103**, 071601 (2009).
- [4] L. M. Barkov and M. S. Zolotarev, "Parity violation in atomic bismuth," *Physics Letters B* **85**, 308–313 (1979).
- [5] C. S. Wood, S. C. Bennett, D. Cho, B. P. Masterson, J. L. Roberts, C. E. Tanner, and C. E. Wieman, "Measurement of parity nonconservation and an anapole moment in cesium," *Science* **275**, 1759–1763 (1997).
- [6] S. G. Porsev, K. Beloy, and A. Derevianko, "Precision determination of weak charge of ^{133}Cs from atomic parity violation," *Phys. Rev. D* **82**, 036008 (2010).

TABLE IX. The excitation energies (cm^{-1}), E1 transition amplitudes (a.u.) and HFS constants (MHz) of Cs with increasing basis.

Orbitals/Basis	Excitation energies				MHFS			E1 amp.		
	$6p_{1/2}$	$6p_{3/2}$	$7s_{1/2}$	$6s_{1/2}$	$6p_{1/2}$	$6p_{3/2}$	$7s_{1/2}$	$6p_{1/2} - 6s_{1/2}$	$6p_{1/2} - 7s_{1/2}$	$6p_{3/2} - 6s_{1/2}$
108(14s12p11d10f8g6h)	10896	11461	18156	2002	251	45	482	4.5888	4.2909	6.4863
119(15s13p12d11f9g7h)	10933	11499	18201	2060	260	46	495	4.5819	4.2881	6.4747
130(16s14p13d12f10g8h)	10977	11544	18257	2110	266	48	506	4.5753	4.2835	6.4616
141(17s15p14d13f11g9h)	11055	11629	18349	2173	273	50	519	4.5632	4.2799	6.4395
152(18s16p15d14f12g10h)	11130	11708	18443	2227	279	50	530	4.5491	4.2733	6.4177
163(19s17p16d15f13g11h)	11169	11749	18503	2263	284	51	536	4.5384	4.2621	6.4039
173(21s19p18d15f13g11h)	11169	11747	18504	2285	288	51	541	4.5377	4.2607	6.4031
178(22s20p19d15f13g11h)	11168	11746	18504	2292	289	51	543	4.5378	4.2604	6.4032
183(23s21p20d15f13g11h)	11168	11746	18503	2298	290	51	544	4.5378	4.2603	6.4033
188(24s22p21d15f13g11h)	11168	11746	18504	2302	290	51	545	4.5378	4.2603	6.4033
193(25s23p22d15f13g11h)	11168	11746	18504	2303	290	51	546	4.5378	4.2603	6.4032

TABLE X. The $E1_{\text{PNC}}^{\text{NSD}}$ amplitudes (in the units of $iea_0 \times 10^{-12} \mu_W$) as a function of basis size.

Basis	$3 \rightarrow 3$	$4 \rightarrow 3$
99(11s10p8d10f8g8h)	1.8103	5.0497
119(15s13p12d11f9g7h)	1.9137	6.0420
129(17s15p14d11f9g7h)	1.9428	6.2450
139(19s17p16d11f9g7h)	1.9683	6.3496
144(20s18p17d11f9g7h)	1.9781	6.3799
149(21s19p18d11f9g7h)	1.9844	6.3973
154(22s20p19d11f9g7h)	1.9899	6.4120
159(23s21p20d11f9g7h)	1.9926	6.4223
164(24s22p21d11f9g7h)	1.9951	6.4348
169(25s23p22d11f9g7h)	1.9959	6.4416
174(26s24p23d11f9g7h)	1.9966	6.4521

[7] M. G. Kozlov, S. G. Porsev, and W. R. Johnson, “Parity non-conservation in thallium,” *Phys. Rev. A* **64**, 052107 (2001).

[8] M. G. Kozlov, S. G. Porsev, and I. I. Tupitsyn, “High-accuracy calculation of $6s \rightarrow 7s$ parity-nonconserving amplitude in Cs,” *Phys. Rev. Lett.* **86**, 3260–3263 (2001).

[9] V. A. Dzuba, J. C. Berengut, V. V. Flambaum, and B. Roberts, “Revisiting parity nonconservation in cesium,” *Phys. Rev. Lett.* **109**, 203003 (2012).

[10] S. G. Porsev, K. Beloy, and A. Derevianko, “Precision determination of electroweak coupling from atomic parity violation and implications for particle physics,” *Phys. Rev. Lett.* **102**, 181601 (2009).

[11] I. A. Zel’dovich, “Electromagnetic interaction with parity violation,” *Soviet Phys. JETP* **6**, 1184–1186 (1958).

[12] W. R. Johnson, M. S. Safronova, and U. I. Safronova, “Combined effect of coherent z exchange and the hyperfine interaction in the atomic parity-nonconserving interaction,” *Phys. Rev. A* **67**, 062106 (2003).

[13] M.S. Safronova, Rupsi Pal, Dansha Jiang, M.G. Kozlov, W.R. Johnson, and U.I. Safronova, “New directions in atomic pnc,” *Nuclear Physics A* **827**, 411c–413c (2009).

[14] B. K. Mani and D. Angom, “Relativistic coupled-cluster calculations of nuclear spin-dependent parity non-conservation in ^{133}Cs , $^{133}\text{Ba}^+$, and $^{133}\text{Ra}^+$,” (2011), arXiv:1104.3473 [physics.atom-ph].

[15] A. Chakraborty and B. K. Sahoo, “High-accuracy nuclear spin dependent parity violating amplitudes in ^{133}Cs ,” (2024), arXiv:2405.19937 [physics.atom-ph].

[16] B.K. Mani, S. Chattopadhyay, and D. Angom, “Rccpac: A parallel relativistic coupled-cluster program for closed-shell and one-valence atoms and ions in fortran,” *Computer Physics Communications* **213**, 136–154 (2017).

[17] S. Chattopadhyay, B. K. Mani, and D. Angom, “Electric dipole polarizability from perturbed relativistic coupled-cluster theory: Application to neon,” *Phys. Rev. A* **86**, 022522 (2012).

[18] S. Chattopadhyay, B. K. Mani, and D. Angom, “Electric dipole polarizability of alkaline-earth-metal atoms from perturbed relativistic coupled-cluster theory with triples,” *Phys. Rev. A* **89**, 022506 (2014).

[19] S. Chattopadhyay, B. K. Mani, and D. Angom, “Triple excitations in perturbed relativistic coupled-cluster theory and electric dipole polarizability of group-iiib elements,” *Phys. Rev. A* **91**, 052504 (2015).

[20] Ravi Kumar, S. Chattopadhyay, B. K. Mani, and D. Angom, “Electric dipole polarizability of group-13 ions using perturbed relativistic coupled-cluster theory: Importance of non-linear terms,” *Phys. Rev. A* **101**, 012503 (2020).

[21] Ravi Kumar, D. Angom, and B. K. Mani, “Fock-space perturbed relativistic coupled-cluster theory for electric dipole polarizability of one-valence atomic systems: Application to Al and In,” *Phys. Rev. A* **106**, 032801 (2022).

[22] B. K. Mani, Palki, Suraj Pandey, and D. Angom, “Perturbed relativistic coupled-cluster calculations of the properties of Ar^{13+} ,” in *Advances in Atomic Molecular Collisions*, edited by Lokesh C. Tribedi (Springer Nature Singapore, Singapore, 2024) pp. 223–240.

[23] M. S. Safronova, W. R. Johnson, and A. Derevianko, “Relativistic many-body calculations of energy levels, hyperfine constants, electric-dipole matrix elements, and static polarizabilities for alkali-metal atoms,” *Phys. Rev. A* **60**, 4476–4487 (1999).

[24] A. Derevianko, W. R. Johnson, M. S. Safronova, and J. F. Babb, “High-precision calculations of dispersion coefficients, static dipole polarizabilities, and atom-wall interaction constants for alkali-metal atoms,” *Phys. Rev. Lett.* **82**, 3589–3592 (1999).

[25] B. K. Mani and D. Angom, “Atomic properties calculated by relativistic coupled-cluster theory without truncation: Hyperfine constants of Mg^+ , Ca^+ , Sr^+ , and Ba^+ ,” *Phys. Rev. A* **81**, 042514 (2010).

[26] B. K. Mani and D. Angom, “The transverse electron-electron interaction in atomic structure calculations,” *Journal of Physics B: Atomic and Molecular Physics* **13**, 2671 (1980).

- [27] B. K. Mani, K. V. P. Latha, and D. Angom, “Relativistic coupled-cluster calculations of ^{20}Ne , ^{40}Ar , ^{84}Kr , and ^{129}Xe : Correlation energies and dipole polarizabilities,” *Phys. Rev. A* **80**, 062505 (2009).
- [28] Geetha Gopakumar, Bhanu Pratap Das, R. K. Chaudhuri, D. Mukherjee, and K. Hirao, “Relativistic coupled-cluster calculations of parity nonconservation in Ba^+ by the sum-over-states approach,” *The Journal of Chemical Physics* **126**, 014301 (2007).
- [29] I. Lindgren and J. Morrison, *Atomic Many-body Theory*, Atoms and Plasmas Series (Springer-Verlag, 1986).
- [30] Ajaya K. Mohanty and E. Clementi, “Kinetically balanced geometric gaussian basis set calculations for relativistic many-electron atoms with finite nuclear size,” *Chemical Physics Letters* **157**, 348–352 (1989).
- [31] P. Jönsson, G. Gaigalas, J. Bieroń, C. Froese Fischer, and I. P. Grant, “New version: Grasp2k relativistic atomic structure package,” *Comp. Phys. Comm.* **184**, 2197 – 2203 (2013).
- [32] Oleg Zatsarinny and Charlotte Froese Fischer, “DBSR_{HF}: A B-spline Dirac-Hartree-Fock program,” *Computer Physics Communications* **202**, 287 – 303 (2016).
- [33] Richard E. Stanton and Stephen Havriliak, “Kinetic balance: A partial solution to the problem of variational safety in dirac calculations,” *J. Chem. Phys.* **81**, 1910–1918 (1984).
- [34] A. Kramida, Yu. Ralchenko, J. Reader, and NIST ASD Team, NIST Atomic Spectra Database (ver. 5.10), [Online]. Available: <https://physics.nist.gov/asd> [2023, March 8]. National Institute of Standards and Technology, Gaithersburg, MD. (2022).
- [35] Andrei Derevianko and Sergey G. Porsev, ““dressing” lines and vertices in calculations of matrix elements with the coupled-cluster method and determination of Cs atomic properties,” *Phys. Rev. A* **71**, 032509 (2005).
- [36] B. K. Sahoo, B. P. Das, and H. Spiesberger, “New physics constraints from atomic parity violation in ^{133}Cs ,” *Phys. Rev. D* **103**, L111303 (2021).
- [37] V. A. Dzuba, V. V. Flambaum, and J. S. M. Ginges, “High-precision calculation of parity nonconservation in cesium and test of the standard model,” *Phys. Rev. D* **66**, 076013 (2002).
- [38] S. A. Blundell, W. R. Johnson, and J. Sapirstein, “Relativistic all-order calculations of energies and matrix elements in cesium,” *Phys. Rev. A* **43**, 3407–3418 (1991).
- [39] S. J. Grunefeld, B. M. Roberts, and J. S. M. Ginges, “Correlation trends in the hyperfine structure for Rb, Cs, and Fr, and high-accuracy predictions for hyperfine constants,” *Phys. Rev. A* **100**, 042506 (2019).
- [40] R. Gupta, W. Happer, L. K. Lam, and S. Svanberg, “Hyperfine-structure measurements of excited s states of the stable isotopes of potassium, rubidium, and cesium by cascade radio-frequency spectroscopy,” *Phys. Rev. A* **8**, 2792–2810 (1973).
- [41] G. Belin, L. Holmgren, and Sune Svanberg, “Hyperfine interaction, zeeman and stark effects for excited states in rubidium,” *Physica Scripta* **13**, 351 (2007).
- [42] W D Williams, M T Herd, and W B Hawkins, “Spectroscopic study of the $7p_{1/2}$ and $7p_{3/2}$ states in cesium-133,” *Laser Physics Letters* **15**, 095702 (2018).
- [43] Vladislav Gerginov, Andrei Derevianko, and Carol E. Tanner, “Observation of the nuclear magnetic octupole moment of ^{133}Cs ,” *Phys. Rev. Lett.* **91**, 072501 (2003).
- [44] G.-W. Truong, J. D. Anstie, E. F. May, T. M. Stace, and A. N. Luiten, “Accurate lineshape spectroscopy and the boltzmann constant,” *Nature Communications* **6**, 8345 (2015).
- [45] E. Arimondo, M. Inguscio, and P. Violino, “Experimental determinations of the hyperfine structure in the alkali atoms,” *Rev. Mod. Phys.* **49**, 31–75 (1977).
- [46] Yunhui He, Jiabei Fan, Liping Hao, Yuechun Jiao, and Jianming Zhao, “Precise measurement of hyperfine structure of cesium $7s_{1/2}$ excited state,” *Applied Sciences* **10** (2020).
- [47] Guang Yang, Jie Wang, Baodong Yang, and Junmin Wang, “Determination of the hyperfine coupling constant of the cesium $7s_{1/2}$ state,” *Laser Physics Letters* **13**, 085702 (2016).
- [48] S. L. Gilbert, R. N. Watts, and C. E. Wieman, “Hyperfine-structure measurement of the $7s$ state of cesium,” *Phys. Rev. A* **27**, 581–582 (1983).
- [49] Arup Chakraborty and Bijaya Kumar Sahoo, “Deciphering core, valence, and double-core-polarization contributions to parity violating amplitudes in ^{133}Cs using different many-body methods,” *The Journal of Physical Chemistry A* **127**, 7518–7533 (2023).
- [50] B. M. Roberts, C. J. Fairhall, and J. S. M. Ginges, “Electric-dipole transition amplitudes for atoms and ions with one valence electron,” *Phys. Rev. A* **107**, 052812 (2023).
- [51] V.A. Dzuba, V.V. Flambaum, A.Ya. Krafnakher, and O.P. Sushkov, “Summation of the high orders of perturbation theory in the correlation correction to the hyperfine structure and to the amplitudes of e1-transitions in the caesium atom,” *Physics Letters A* **142**, 373–377 (1989).
- [52] M. S. Safronova, U. I. Safronova, and Charles W. Clark, “Magic wavelengths, matrix elements, polarizabilities, and lifetimes of Cs,” *Phys. Rev. A* **94**, 012505 (2016).
- [53] George Toh, Amy Damitz, Nathan Glotzbach, Jonah Quirk, I. C. Stevenson, J. Choi, M. S. Safronova, and D. S. Elliott, “Electric dipole matrix elements for the $6p^2P_J \rightarrow 7s^2S_{1/2}$ transition in atomic cesium,” *Phys. Rev. A* **99**, 032504 (2019).
- [54] Amy Damitz, George Toh, Eric Putney, Carol E. Tanner, and D. S. Elliott, “Measurement of the radial matrix elements for the $6s^2s_{1/2} \rightarrow 7p^2p_J$ transitions in cesium,” *Phys. Rev. A* **99**, 062510 (2019).
- [55] Maxwell D. Gregoire, Ivan Hromada, William F. Holmgren, Raisa Trubko, and Alexander D. Cronin, “Measurements of the ground-state polarizabilities of Cs, Rb, and K using atom interferometry,” *Phys. Rev. A* **92**, 052513 (2015).
- [56] Jason M. Amini and Harvey Gould, “High precision measurement of the static dipole polarizability of cesium,” *Phys. Rev. Lett.* **91**, 153001 (2003).
- [57] B. M. Patterson, J. F. Sell, T. Ehrenreich, M. A. Gearba, G. M. Brooke, J. Scoville, and R. J. Knize, “Lifetime measurement of the cesium $6P_{3/2}$ level using ultrafast pump-probe laser pulses,” *Phys. Rev. A* **91**, 012506 (2015).
- [58] Ivan S. Lim, Peter Schwerdtfeger, Bernhard Metz, and Hermann Stoll, “All-electron and relativistic pseudopotential studies for the group 1 element polarizabilities from K to element 119,” *The Journal of Chemical Physics* **122**, 104103 (2005).
- [59] A. Chakraborty and B. K. Sahoo, “High-precision electric dipole polarizabilities of the clock states in ^{133}Cs ,” *Phys. Rev. A* **108**, 042818 (2023).
- [60] A. Derevianko, W. R. Johnson, M. S. Safronova, and J. F. Babb, “High-precision calculations of dispersion coefficients, static dipole polarizabilities, and atom-wall interaction constants for alkali-metal atoms,” *Phys. Rev. Lett.* **82**, 3589–3592 (1999).
- [61] E. Iskrenova-Tchoukova, M. S. Safronova, and U. I. Safronova, “High-precision study of Cs polarizabilities,” *Journal of Computational Methods in Sciences and Engineering* **7**, 521–540 (2009).
- [62] Robert W. Molof, Henry L. Schwartz, Thomas M. Miller, and Benjamin Bederson, “Measurements of electric dipole polarizabilities of the alkali-metal atoms and the metastable noble-gas atoms,” *Phys. Rev. A* **10**, 1131–1140 (1974).

- [63] M. S. Safronova and Charles W. Clark, “Inconsistencies between lifetime and polarizability measurements in Cs,” *Phys. Rev. A* **69**, 040501 (2004).
- [64] H. L. Zhou and D. W. Norcross, “Improved calculation of the quadratic stark effect in the $6P_{3/2}$ state of Cs,” *Phys. Rev. A* **40**, 5048–5051 (1989).
- [65] L. R. Hunter, D. Krause Jr., S. Murthy, and T. W. Sung, “Precision measurement of the stark shift of the cesium d lines,” *Phys. Rev. A* **37**, 3283–3292 (1988).
- [66] L.R. Hunter, D. Krause, K.E. Miller, D.J. Berkeland, and M.G. Boshier, “Precise measurement of the stark shift of the cesium d1 line,” *Optics Communications* **94**, 210–214 (1992).
- [67] W.A. van Wijngaarden and J. Li, “Polarizabilities of cesium s, p, d, and f states,” *Journal of Quantitative Spectroscopy and Radiative Transfer* **52**, 555–562 (1994).
- [68] S. C. Bennett, J. L. Roberts, and C. E. Wieman, “Measurement of the dc stark shift of the $6s \rightarrow 7s$ transition in atomic cesium,” *Phys. Rev. A* **59**, R16–R18 (1999).
- [69] V. G. Domelunksen, “Polarizability of ^{133}Cs atom in the $7^2P_{1/2}$ and $7^2P_{3/2}$ states,” *Optics and Spectroscopy* **54**, 565–567 (1983).
- [70] E. A. Uehling, “Polarization effects in the positron theory,” *Phys. Rev.* **48**, 55–63 (1935).
- [71] L. Wayne Fullerton and G. A. Rinker, “Accurate and efficient methods for the evaluation of vacuum-polarization potentials of order $z\alpha$ and $z\alpha^2$,” *Phys. Rev. A* **13**, 1283–1287 (1976).
- [72] S. Klarsfeld, “Analytical expressions for the evaluation of vacuum-polarization potentials in muonic atoms,” *Physics Letters B* **66**, 86–88 (1977).
- [73] V. M. Shabaev, I. I. Tupitsyn, and V. A. Yerokhin, “Model operator approach to the lamb shift calculations in relativistic many-electron atoms,” *Phys. Rev. A* **88**, 012513 (2013).
- [74] V.M. Shabaev, I.I. Tupitsyn, and V.A. Yerokhin, “Qedmod: Fortran program for calculating the model lamb-shift operator,” *Computer Physics Communications* **189**, 175–181 (2015).
- [75] Ravi Kumar, S. Chattopadhyay, D. Angom, and B. K. Mani, “Relativistic coupled-cluster calculation of the electric dipole polarizability and correlation energy of Cn, Nh^+ , and Og: Correlation effects from lighter to superheavy elements,” *Phys. Rev. A* **103**, 062803 (2021).